GEORGE BROWN PRESS
JOURNALS, BOOKS & PROCEEDINGS

Journal of Medicine and Life Sciences

Article

Computational and Experimental Drug Discovery Targeting the Glycolytic Pathway in Methicillin-Resistant Staphylococcus Aureus

Ziyao Liu [1,*]

[1] School of biochemistry, University of Edinburgh, Edinburgh, UK
* Correspondence: Ziyao Liu, School of biochemistry, University of Edinburgh, Edinburgh, UK

Abstract: This dissertation studies the metabolic pathways of methicillin-resistant Staphylococcus aureus (MRSA), focusing on the enzyme MRSaFBA. It highlights the enzyme's potential as a therapeutic target for antibacterial strategies. By employing biophysical techniques including Dynamic Light Scattering (DLS) and Thermal Denaturation Analysis (TDA), the study provides new insights into the structural stability and aggregation behavior of MRSaFBA under various conditions. The research also demonstrates improvements in protein production and purification processes, enhancing the yield and purity of MRSaFBA and enabling more precise biochemical characterization. Furthermore, enzymatic assays confirm the enzyme's sensitivity to environmental factors and inhibitors, underscoring its potential as a drug target. The study also incorporates molecular docking to understand the interaction mechanisms of potential inhibitors, laying a foundation for the development of MRSaFBA-HCA site.

Keywords: drug discovery; methicillin-resistant Staphylococcus aureus; fructose-1,6-bisphosphate aldolase; molecular docking; enzymatic assays; active site binding

1. Introduction

1.1. Introduction to Yellow Staphylococci

Staphylococcus aureus (SA) is a Gram-positive, plasma coagulase- positive opportunistic pathogen that adheres and colonises various parts of the human body [1], and when the conditions are right, it can cause infections at various sites, such as infections of the bloodstream, soft tissues of the skin and the lower respiratory tract. In addition, the organism is also closely associated with medical device-associated infections and deep-seated infections, such as catheter-associated infections, osteomyelitis, endocarditis, etc. [2]. In recent years, due to the inappropriate use of antibiotics and the evolution of bacteria themselves, drug resistance of SA has been increasing, and multidrug-resistant strains are emerging, especially the emergence of methicillin-resistant Staphylococcus aureus (MRSA), which can lead to the host being more susceptible to chronic and persistent, recurrent infections The emergence of MRSA can lead to increased susceptibility of hosts to chronic, persistent, recurrent infections and even outbreaks of invasive infections with high mortality [3], posing a great challenge to the global public health system.

The pathogenesis of MRSA is complex and multifaceted. Firstly, MRSA can produce a large number of toxins through virulence factors, such as proteases, enterotoxins, haemolysins, etc. These toxins can attack the human immune system and lead to a variety of serious diseases, such as scalded skin syndrome, staphylococcal food-borne disease and toxic shock syndrome [4]. Secondly, MRSA has acquired multi-drug resistance with multiple complex resistance mechanisms, including decreased permeability of cell membranes, activation of the exocytosis system, production of β- lactamases, transmission of resistance genes, and formation of bio- permeable membranes [5-9], which have rendered

Received: 07 April 2025
Revised: 12 April 2025
Accepted: 05 May 2025
Published: 10 May 2025

the majority of antibiotics ineffective against MRSA in the clinic. Therefore, the number of antibiotics available for the treatment of MRSA infection is very limited, and the glycopeptide antibiotics represented by vancomycin are still the first-line drugs for the treatment of MRSA infection, and there are many newly developed drugs against MRSA infection in recent years, but the speed of bacterial resistance is much faster than the speed of antibiotic research and development, which leads to the emergence of drug-resistant bacteria in a very short period of time after the entry into the clinic, and the toxic side-effects of antibiotics themselves, which leads to the emergence of drug- resistant bacteria and the development of antibiotics. However, because the rate of bacterial resistance far exceeds the rate of antibiotic development, resulting in the emergence of drug-resistant bacteria within a very short time of clinical use, and because antibiotics have their own toxicity and side effects, their use in the clinic is very limited [10].

1.2. Overview of MRSA Pathogenicity Studies

Staphylococcus aureus (S. aureus) is one of the most prevalent food- borne pathogens worldwide [11,12]. MRSA has now become a major pathogen in hospitals and community settings, leading to prolonged hospitalisation and increased mortality. The most important reason for MRSA's resistance to penicillin is its possession of a gene encoding a penicillin-binding protein that blocks the inhibitory effect of penicillin (β-lactam) on the cross-linking of peptidoglycan [13-15].

1.3. Pathogenic Factors of MRSA

Pathogenesis generally results from a combination of virulence factors. Biofilm formation helps the strain persist in the environment or host and increases resistance to antibiotics and host defenses [16,17]. Biofilm formation occurs in four stages: surface attachment, accumulation, maturation, and dissemination. Systemic MRSA infections often begin when bacteria breach the skin barrier or form biofilms on medical devices. Therefore, inhibiting biofilm formation is considered a key strategy in treating MRSA infections [18]. In the blood or tissues, MRSA can attack and eliminate immune cells via haemolysins or enter the cells and subsequently infect the whole body. Neutrophils are the most common leukocytes and play an important role in inhibiting pathogenic infections, but MRSA can evade clearance by the host immune system by inhibiting the phagocytosis and killing mechanisms of neutrophils and eliminating phagocytes and other immune cells. At the same time, S. aureus secretes cofactors that activate host zymogens and enzymes that degrade tissue components, and these enzymes help the bacteria to obtain nutrients, survive and spread [19]. S. aureus can produce a variety of toxins to enhance its pathogenicity, including α-, β-, γ- and δ-hemolysins that can lyses erythrocytes by forming pores in the host cell membrane or lysing cell wall components [20]. Phenololysis-regulating peptides are important, invasive virulence factors in S. aureus, and are small peptides with an amphiphilic α-helix structure and surfactant-like characteristics, playing multiple roles in S. aureus pathogenesis, including lysis of eukaryotic cells, periplasmic membrane formation, and immunomodulation [21]. Enterotoxins secreted by S. aureus frequently contaminate food and are not easily destroyed due to resistance to heat, freezing, and drying, often causing foodborne illness with symptoms such as nausea, vomiting, and diarrhoea [22]. Toxic shock syndrome toxin 1 does not cause vomiting but stimulates large-scale release of pro-inflammatory factors from host T cells and macrophages, leading to toxic shock syndrome symptoms such as high fever, rash, desquamation, hypotension, hypovolemic shock, and even organ failure or death [23].

1.4. MRSA Colonisation and Infection

Staphylococcus aureus colonises the nasal cavity and is present in approximately 30% of asymptomatic healthy people [24]. Nasal carriage of S. aureus is a common cause of infection, which can occur when the host is immunocompromised or during surgery.

Therefore, rapid screening and decolonisation of the nasal cavity for S. aureus in patients undergoing surgery may be effective in reducing the likelihood of surgical site infections [25]. Huang et al. found that MRSA-positive patients who underwent MRSA decolonisation for 6 months after discharge from the hospital had a 17% reduction in the likelihood of developing MRSA infections compared to those who did not undergo MRSA decolonization [25,26]. A 6-year survey of 138 asymptomatic healthy volunteers found that 18.8 % of volunteers had MRSA strains colonising their throats for more than 3 years [27]. The correlation between MRSA colonisation of the throat and MRSA colonisation of the nasal cavity needs to be taken into account when decolonising [28]. Yang et al. investigated the rate of MRSA colonisation at four body sites in MRSA-infected patients and found that 25 % of the patients were colonised by MRSA in the nasal cavity, 6 % in the axilla, 17 % in the groin, and 13 % in the rectal region [29]. In addition, MRSA has been shown to persistently colonise the gut and has been found to be carried in the gut of healthy newborns [30]. Gries et al. found that persistent colonisation of the gut by MRSA may be associated with the mucus layer of the cecum, which is not readily penetrated by antibiotics, and that MRSA can form a biofilm in the mucus layer that makes it less susceptible to killing by antibiotics [31]. Small bowel colitis caused by MRSA was first reported in Europe in 1961, and MRSA may cause antibiotic-associated diarrhoea [32,33]. MRSA colonising the gut may also cause infections in other more distant tissue wounds, as it can reach other parts of the host and change from a colonised to a pathogenic state [34,35]. MRSA infections have become a global health threat and healthcare burden because of its ability to colonise different parts of the host and its potential risk of infecting the host and causing disease [36]. MRSA infection in the community often causes skin infections, but can also lead to pneumonia and, in extreme cases, bacteraemia; in the hospital setting MRSA infections can lead to

more severe bacteraemia, pneumonia, surgical site infections and other infections. In the hospital setting MRSA infection can lead to more serious bacteraemia, pneumonia, and surgical site infections. Surgical site infections after neonatal abdominal surgery have been associated with MRSA colonisation as well as prolonged antibiotic use and hospitalisation [37]. After analysing clinical data from children hospitalised for 10 years, the main pathogen for skin and soft tissue infections in children is MRSA [38]. Bacteraemia is also a common symptom of infection and there is a high mortality rate associated with MRSA [39]. Abebe et al [40] cultured and analysed blood from patients with suspected sepsis over a six-year period and found that Staphylococcus aureus was the most common bacterium, which also contained MRSA, and MRSA-associated bacteraemia has been seen in a number of hospitals, and is often associated with catheters or other inbuilt catheters in dialysis patients [41-43]. Hospital-acquired pneumonia and ventilator-associated pneumonia are two common types of pneumonia in hospitalised patients, and S. aureus, especially MRSA strains, is one of the main pathogens causing these two types of pneumonias, which are associated with a significantly higher morbidity and mortality rate than community-acquired pneumonia. Therefore, when decolonising MRSA or treating MRSA-induced infections, the site of infection should be considered.

1.5. Factors Influencing the Virulence of Methicillin-Resistant Staphylococcus Aureus

The major influences on the virulence of methicillin-resistant Staphylococcus aureus (MRSA) are the result of a series of toxin adhesion and immune escape based on multiple factors. Toxins and virulence of methicillin-resistant S. aureus are directly related to the coding status of mobile genetic factors [44-46]. Mobile genetic factors can encode toxins, including hyperantigenic toxic shock syndrome toxins, interleukins, etc. [47- 50] PVL is a potent exotoxin that can be secreted by methicillin-resistant S. aureus, which is capable of causing leukocytolysis and is particularly potent in lysing neutrophils [51]. There is a direct relationship between PVL and early skin infections, such as surgical incisions, trau-

matised surfaces, subcutaneous infections and other septic lesions [52]. This molecule possessed by methicillinresistant Staphylococcus aureus is the main discriminatory site for the differentiation of community-acquired and hospital-acquired infection strains [53]. In community-acquired strains, predominantly USA300 strains [54], the PVL gene is highly expressed, whereas hospital-acquired strains have relatively low levels of PVL expression [55]. Therefore, to a certain extent, it can be assumed that community-acquired strains have a higher level of expression of virulence- producing genes than hospital-acquired strains, and it can be clinically assumed that community-acquired strains should be more virulent.

When methicillin-resistant Staphylococcus aureus comes from hospital-acquired infections, many strains contain specific toxin genes, which is also an important reference mark to classify their lineage. Among them, the TSST and CC30/USA200 lineages are the most typical representatives [56]. Isolated CC30 carries auxiliary gene regulator C mutations and HLA locus mutations that reduce the acute virulence of methicillin-resistant S. aureus [57]. Among the contemporary clonal strains of CC30, EMRSA-16 is the most common. In this strain, auxin regulator C is mutated, reducing auxin regulator activity while producing higher δ-toxin and a large number of phenol-soluble regulatory proteins [58]. Phenol- soluble regulatory proteins are the main members of the S. aureus fungal toxin PSM, but are distinct from other PSM family members. This toxin is encoded on MGE [59], so it can represent a specific spectrum of methicillin- resistant S. aureus. PSM is also an amphiphilic polypeptide, which effectively enhances lysis of certain bacterial cells. Among them, neutrophils and erythrocytes are more sensitive. Therefore, this substance also increases the virulence of S. aureus infection becoming an important risk factor [60].

Surface proteins play an important role in the infection phase of S. aureus. This protein not only plays a key role in the metabolism of the bacterial cell wall, but also participates in host-bacterial conjugation and accelerates immune escape. It also has an impact on the rate of bacterial aggregation and biofilm formation. Most of the surface protein code is located in the core genome. Accessory gene regulator (Agr) is a worldwide regulatory system found in some Gram-positive bacteria, especially Staphylococcus aureus. It is necessary for the Agr system to regulate its virulence factors such as toxins, surface proteins and other effectors. In previous studies, Agr was thought to have a virulence modulating effect, promoting toxin production to the detriment of surface protein expression. However, recent studies have suggested that Agr may also promote surface protein expression processes, which may be related to changes in conditions [61].

1.6. Biofilms of Methicillin-Resistant Staphylococcus Aureus (MRSA)

Bacterial clusters attached to the surface of the extracellular matrix are considered to be biofilms of methicillin-resistant Staphylococcus aureus. In the past, it has been considered that staphylococci are good carriers of biofilm formation because the surface molecules produced by staphylococci are effective in accessing the formation of the extracellular matrix [62]. Due to their presence, biofilms are also effective in reducing antibiotic and host immune attack on both biotic and abiotic surfaces to which bacteria attach. It is easy to see that biofilms contribute to the infection and colonisation of methicillin-resistant S. aureus.

1.7. Main Influencing Factors on Colonisation of Methicillin-Resistant S. Aureus

Methicillin-resistant Staphylococcus aureus is widely parasitised in medical waste, reused medical equipment, making it an intermediate source of methicillin-resistant Staphylococcus aureus infections, but ultimately such infections come from patients or healthcare workers carrying methicillin-resistant Staphylococcus aureus [63]. The respiratory tract is the most important host site for methicillin-resistant Staphylococcus aureus, and the nasal cavity contains the highest level of methicillin- resistant Staphylococcus aureus in the human body. In addition to the nasal cavity, which is capable of carrying

methicillin-resistant Staphylococcus aureus, which was discovered in 1931 with irrigation of the patient's fingertips, there are a number of other sites where Staphylococcus aureus can colonise, such as the pharynx and the perineum, which are not the main sources of methicillin-resistant Staphylococcus aureus infections. A survey of patients with methicillin-resistant S. aureus infection found that 1/5 of them were persistent carriers of methicillin-resistant S. aureus in the nasal cavity, while 30% were intermittent carriers of methicillin-resistant S. aureus, but half of the patients never experienced methicillin-resistant S. aureus colonisation [64]. The percentage of carriers in patients is also directly related to race, while certain diseases may also increase the rate of carriage. This can be seen that the host's own physical condition is an important influence on methicillin-resistant S. aureus colonisation, but exactly how it has an effect and its molecular mechanism has not been a clear conclusion so far.

1.8. Effect of Drug Resistance of Methicillin-Resistant Staphylococcus Aureus

Some studies have confirmed that methicillin-resistant Staphylococcus aureus resistance is associated with the mutation level of the SCCmec gene [65]. Five subtypes of SCCmec have been identified in the available studies. MecA gene can be seen in the shadow of many types. The product of this gene is a penicillin-binding protein with low affinity for penicillin. This is the main mechanism of methicillin resistance in methicillin-resistant Staphylococcus aureus and organises bacterial cell wall synthesis [66]. SCCmec genes may be related to other staphylococci in origin or may have been acquired by horizontal transfer from the same genus, S. aureus. In addition, up-regulation of the expression of the bla gene encoding a β- lactamase and the fem gene encoding a gene essential for methicillin resistance also affects the internal drug properties of methicillin. It can be concluded that methicillin resistance of methicillin-resistant Staphylococcus aureus to methicillin drug is the result of multiple genes acting together [67]. Environmental factors are also important influences on methicillin resistance. The presence of SCCmec type II can usually be detected by isolation of hospital-acquired methicillin-resistant Staphylococcus aureus (MRSA) strains, whereas community-acquired MRSA strains can be detected. The presence of SCCmec type II can be detected by isolation of hospital-acquired MRSA strains and community-acquired MRSA strains. Among S. aureus strains, the presence of SCCmecIV is usually detected [68].

1.9. Methicillin-Resistant S. Aureus and Wound Infections

Methicillin-resistant Staphylococcus aureus is more likely to colonise or become infected in the presence of a wound, which can make clinical management difficult. In patients with chronic infections, wounds are an important site for bacterial survival. Methicillin-resistant Staphylococcus aureus was detected in up to 40% of the wounds collected from diabetic foot patients, and it is also an important pathogen that causes diabetic foot wound infections. The foot is also an important pathogen that causes foot infections in patients with diabetic foot disease. In some recent studies, infectious agents, mainly methicillin-resistant Staphylococcus aureus, were present in pressure ulcer wounds and showed characteristics of opportunistic infections. Also, the presence of bacterial biofilms can be detected [69]. To date, the most common sites of community-acquired methicillin-resistant Staphylococcus aureus infections are the skin and soft tissues. In addition, community-acquired methicillin-resistant Staphylococcus aureus strains have been found to have cases of bone, joint, and respiratory tract infections. Co-infections prolong clinical care and complicate treatment. Controlling MRSA infections while addressing drug resistance and reducing infection rates is a key clinical priority.

1.10. Treatment Options for Methicillin-Resistant Staphylococcus Aureus Infections

Vancomycin is the treatment of choice when severe methicillin- resistant Staphylococcus aureus infections occur, but this drug is not perfect. Vancomycin, when used in

large quantities, is prone to the emergence of hypo-susceptible strains, reduced clinical efficacy, and high-dose nephrotoxicity, all of which can affect its use in clinical work. In the US FDA data, five antibiotics are specifically approved for the treatment of methicillin-resistant Staphylococcus aureus infections. These include linezolid, daptomycin, tigecycline, travancin, and ceflorin [70].

Linezolid, a member of the oxazolidinone class of antimicrobials, contains 100% bioavailability and has good tissue penetration and effective distribution in the skin and soft tissues of diabetic patients. In some studies, linezolid has been shown to be effective in skin and associated soft tissue involvement associated with methicillin-resistant Staphylococcus aureus infections. The number of resistance reports associated with linezolid is low, so it is unknown whether it causes resistance in methicillin-resistant S. aureus.

Daptomycin is a cyclic lipopeptide, which has a significant effect on Gram-positive bacteria represented by methicillin-resistant S. aureus and vancomycin-resistant enterococci. In the currently available guideline recommendations, the use of daptomycin IV can be used as an alternative treatment for patients with bacteraemia caused by methicillin-resistant S. aureus. In the opinion of some scholars, it is even possible to increase the dosage of the drug to improve its therapeutic effect. However, daptomycin is associated with some adverse effects, including rhabdomyolysis, peripheral neuropathy, and eosinophilic pneumonia. In some studies, it has been noted that serum creatine phosphokinase is elevated after daptomycin treatment and can cause drug myopathy. Therefore, the frequency of daptomycin administration should be strictly limited to less than once a day.

Tigecycline is a semisynthetic derivative of dimethylaminotetracycline with a large antibacterial spectrum. The therapeutic efficacy of tigecycline is not indicated in the latest treatment protocols for methicillin-resistant S. aureus infections because the FDA safety statement indicates that the addition of tigecycline to the treatment regimen of more severe patients results in a higher overall mortality rate than conventional therapy. Although there is no significant difference in actual efficacy between tigecycline and other alternatives in skin infections, tigecycline can often serve as a second- or third-line agent in the treatment of methicillin-resistant S. aureus infections when alternatives are not available.

Travancin is a parenteral lipoglycopeptide that is recommended by FDA guidelines to be administered once daily for the treatment of skin infections caused by methicillin-resistant Staphylococcus aureus, and was first approved in June 2013 for the treatment of nosocomialacquired pneumonia in gram-positive organisms with predominantly methicillin-resistant Staphylococcus aureus infections. It has been approved in European guidelines, but use is explicitly limited to patients with confirmed or suspected methicillin-resistant S. aureus infection [71].

Ceflorin was the first cephalosporin approved by the FDA for the treatment of methicillin resistant Staphylococcus aureus, and was found to be well tolerated with a low incidence of adverse events in clinical trials.

1.11. MRSaFBA as a Target

In the face of the continued threat and evolution of MRSA (Methicillin- resistant Staphylococcus aureus), the scientific community is eagerly exploring innovative drug intervention strategies, turning the spotlight on the S. aureus-specific 1,6-diphosphofructuran aldolase (SaFBA), a key enzyme class considered as an emerging pharmacological target. SaFBA is a member of the class II 1,6-bisphosphofructuran aldolases (FBAs) SaFBA belongs to the family of class II 1,6-bisphosphate fructose aldolases (FBAs), which together with class I FBAs form the two pillars of this metabolic process.

At the biochemical level, the core function of both class I and class II FBAs is to catalyse the reversible aldol condensation reaction between dihydroxyacetone phosphate (DHAP) and glyceraldehyde 3-phosphate (G3P) to produce the essential fructose 1,6-

bisphosphate (FBP) [72]. However, the two are quite different in their catalytic mechanisms: class I FBAs rely on lysine residues to construct nucleophilic enamines as a means to drive the conversion of DHAP [73], whereas class II FBAs, such as SaFBA, cleverly utilize Zn(II) cations as catalysts to stabilise the DHAP enolate intermediates in the reaction, thereby efficiently completing the aldol condensation.

Further in-depth analyses revealed that these two classes of FBAs also have significant structural differences, especially in the position of the key amino acid side chain responsible for the proton transfer and addition reaction, a difference that not only reflects their evolutionarily independent pathways, but also provides unique binding sites for drug design. It is worth noting that the possession of these two classes of FBAs in organisms is also differentiated: higher organisms, such as humans, are equipped with only class I FBAs [74]; protozoa, bacteria, fungi, and blue-green algae generally rely on class II FBAs for metabolism [75]; and a few organisms have both, demonstrating the diversity and complexity of enzyme distribution in nature.

Therefore, an in-depth study of the unique properties of SaFBA, a class II FBA, is not only expected to bring new hope for the treatment of drug- resistant bacteria, such as MRSA, but may also open up new avenues for a broader range of therapeutic strategies for infectious diseases. The summary table of the mechanism of reaction is shown in Table 1.

Table 1. The summary table of the mechanism of reaction.

Aspect	Description	Exploitable Features for Drug Design
Enzyme Class	SaFBA belongs to class II bisphosphofructuran aldolases (FBAs).	Class II specific characteristics not found in class I, making it a unique target
Catalytic Mechanism	Utilizes Zn(II) cations to stabilize DHAP enolate intermediates	Zn(II) binding site can be targeted to inhibit activity
Reaction Catalyzed	Reversible aldol condensation between DHAP and G3P to produce FBP	Interference with substrate binding or transition state stabilization can disrupt function
Key Structural Features	Significant structural differences in the position of key amino acid side chains responsible for proton transfer	Unique amino acid residues and structural configuration can be targeted for selective inhibition
Organism Distribution	Higher organisms (humans) have class IFBAs; protozoa, bacteria, fungi, and blue-green algae rely on class II FBAs	Selectivity for class II FBAs reduces the risk of affecting human enzymes
Drug Resistance Potential	Targeting SaFBA can overcome traditional antibiotic resistance mechanisms found in MRSA	Development of inhibitors that specifically bind to SaFBA, circumventing existing resistance
Therapeutic Potential	SaFBA is a promising target for treating drug-resistant bacteria like MRSA and potentially other infectious diseases	Exploiting SaFBA can provide a novel treatment avenue distinct traditional antibiotics

1.12. Options and Prospects for MRSaFBA

In view of MRSA's resistance to multiple antibiotics, it has become imperative to find new therapeutic targets. MRSaFBA, as a key component of the MRSA metabolic pathway, has the potential to become a new target for drug action. By inhibiting the activity of FBA, we can block the energy metabolism pathway of MRSA and thus achieve the purpose of

treating the infection. It has been found that single gene knockdown attempts of the E. coli fbaA gene (class II) have proved unsuccessful, whereas knockdown of the fbaB gene (class I) is feasible [76]. Significant expression levels of class I FBA in E. coli were observed only in the presence of glucose substrate, suggesting that class I FBA is only conditionally present. JM2087 was reported to be an E. coli strain with 11 mutations (including the fbaA-1 gene), but the exact cause of its survival and the nature of the mutation in the fbaA- 1 gene are not known [77]. Studies on the fba gene in E. coli are consistent with those on M. tuberculosis in that only class I enzymes are observed under hyperaerobic conditions, whereas class II MtFBA is expressed alone at high levels under hypoxic conditions [78]. Attempts to replace the wild- type fba (class II) gene in Mycobacterium tuberculosis with a deleted allele by a two-step homologous recombination procedure also proved to be unsuccessful. Since the structure of each family member of class II has been determined, although PGH and its analogues are potent inhibitors of FBAs due to their structural similarity to DHAP, this similarity also makes them potent inhibitors of human class I FBAs, thus making them nonspecific and unsuitable for drug development. In addition, Capodagli et al. developed a chemical scaffold, 8-hydroxyquinoline-2-carboxylic acid, for inhibition used in the treatment of tuberculosis and other bacterial and protozoan infections. Although HCA is able to exploit the dynamic flexibility of the Z-ring in class IIa FBAs to form hydrophobic pockets and bind to them, this property is not fully conserved between class IIa and class IIb FBAs. Significant differences in the structural features of the Z-ring and its surroundings in class IIb FBAs compared to that of class IIa limit the general applicability of HCA to class IIb FBAs. It was shown that the inhibition of class IIa FBAs in M. tuberculosis (Mycobacterium tuberculosis) by HCA was non-competitive, whereas the inhibition of class IIb FBAs in S. aureus (Staphylococcus aureus) was of a mixed type and the inhibition constants (Ki) were almost 8-fold weaker. This difference in inhibition patterns suggests that the inhibitory effect of HCA is strongly dependent on the specific subclass structure of FBA. Due to the structural differences between different FBA subclasses, HCA may not be able to act as a broad- spectrum inhibitor to inhibit all types of FBAs. In particular, the inhibitory efficacy of HCA may be greatly reduced for those FBA subclasses that have weak Z-loop dynamics or significantly different structural features. In order to develop efficient inhibitors capable of targeting multiple FBA subclasses simultaneously, an in-depth understanding of the structural differences between different FBA subclasses and how these differences affect the binding and inhibitory effects of small molecule inhibitors is required. This may add to the complexity and challenge of drug design. Therefore, MRSaFBA is highly desirable as a good research target.

In addition, with the in-depth analysis of the molecular structure and functional mechanism of MRSaFBA, we can foresee that FBA-based inhibitors or targeted therapies will become an important means to achieve precision medicine and personalised treatment. By detecting specific mutations or expression levels of MRSaFBA in patients, doctors can tailor a more targeted treatment plan to improve therapeutic efficacy and reduce unwanted side effects of drugs. The research on MRSaFBA will accelerate the research and development process of new antibacterial drugs. Based on the unique structure and function of FBA, researchers can design inhibitors with high selectivity and specificity. These novel drugs can not only effectively inhibit the growth of MRSA, but also reduce the impact on other non-pathogenic microorganisms, thus reducing ecosystem damage. In addition, with the continuous advancement of technology, we can expect these novel antimicrobial drugs to achieve continuous optimisation and innovation in terms of efficacy, safety, and cost-effectiveness. The research on MRSaFBA will promote the cross-fertilisation of several disciplines, such as microbiology, pharmacology, molecular biology, structural biology, and so on. This multidisciplinary collaboration will not only help us understand the biological properties and mechanism of action of MRSaFBA more comprehensively, but will also promote the application of new technologies in drug discovery and development. For example, potential FBA inhibitors can be rapidly identified using

high-throughput screening techniques; the structure of inhibitors can be optimised to improve their activity and stability using structural biology and computer simulation techniques; and the efficacy and safety of drugs can be predicted using artificial intelligence and big data analytics techniques, etc. As a highly drug-resistant pathogenic bacterium, MRSA poses a serious threat to the safety of global public health. Through in-depth research on MRSAFBA and the development of novel therapeutic drugs, we can effectively curb the spread and infection of MRSA, thereby reducing its harm to human health. This will help consolidate and enhance global public health security and safeguard human health and lives. In addition, these findings will provide useful reference and inspiration for the study of other drug-resistant bacteria, and promote the progress and development of the entire anti-infective field. The study of MRSAFBA will also provide us with important clues to reveal the new mechanism of MRSA drug resistance. By comparing the variation of FBA in different strains and its relationship with drug resistance, we can identify new drug resistance genes or drug resistance pathways, and accordingly develop more effective response strategies. These strategies may include combinations, alternations, dose adjustments, and other modalities aimed at improving therapeutic efficacy and delaying the emergence and development of drug resistance.

1.13. Research Question

The aim of this study is to contribute to the effort against traditional techniques used in antibiotic resistance and to aid in the development of effective remedies against MRSA as well as other infectious diseases. The current study will cover the production and purification of MRSaFBA with a view to exploring its unique structural as well as functional features. Dynamic Light Scattering (DLS), Thermal Denaturation Assay (TDA), enzyme assays, and molecular docking techniques will be employed. Lastly, this research will then seek newer drug intervention mechanisms targeting MRSA specifically by looking into its 1,6-bisphosphate fructuronase which is peculiar.

2. Material and Methods

2.1. Production and Purification of MRSaFBA.

Two separate methodologies were employed in the production and purification of MRSa FBA, each yielding a batch of protein with different purity and activity characteristics.

2.1.1. Batch-1 Production and Purification

The FBA expression vector for a methicillin-resistant strain of Staphylococcus aureus (MRSaFBA) was provided by University of Edinburgh. The pET3a-C41 DE3 plasmid was transformed into E.coli BL21 (DE3) by heat-shock. At 42˚C for 45 seconds, followed by 5 minutes on ice. Following this, 900 μL of SOC was added and the sample incubated shaking (250 r.p.m.) at 37 °C for 45 minutes and then inoculated into 25 mL of LB broth containing 100 μg/mL carbenicillin and incubated shaking at 260 r.p.m. at 37 °C overnight. Cells were first pelleted from LB medium and then transferred to 500 mL of 2×TY medium containing 100 μg/mL carbenicillin. Cells were grown to an OD600 of 0.8, then cold shocked under 4 °C for 1 hour. Following this, IPTG was added to a final concentration of 0.4 mM IPTG induce the over-expression of the MRSaFBA, and the culture was incubated shaking at 250 r.p.m at 18 °C overnight. Cells were harvested by centrifugation at 6,000 × g for 20 minutes. and flash frozen with liquid nitrogen, and stored at -70°C.

2.1.2. Batch-1 Lysis

Cell pellets from a 1 L culture were resuspended to 10% wt/vol in 50 mL of Purification Buffer (50 mM TEA, 300 mM NaCl, 10% glycerol, pH 8.0). One EDTA-free Protease Inhibitor Cocktail Tablet (Roche) was added to the suspension. The cells were lysed by a single passage through a Constant Systems TS Bench-top Cell Disruptor set to 25,000 psi.

Following lysis, the cell debris was removed by centrifugation at 20,000 rpm for 60 minutes at 4°C using a JA-25.50 rotor. The resulting supernatant was collected and filtered through a 0.45 μm filter. The clarified lysate was then loaded onto an IMAC column (specify size and type here for clarity on capacity, yield potential, and flow rates). At each stage of the purification process, a 100 μL sample was collected for subsequent comparative analysis.

During the initial purification process, four experimental steps were performed to achieve a relatively pure MRSaFBA protein. The MRSaFBA protein, which was tagged with a His-tag, underwent the first stage of purification using Immobilized Metal Affinity Chromatography (IMAC). The specific procedure was as follows: the filtered MRSaFBA solution was loaded onto a 5 mL HisTrap FF IMAC fast flow column, which had been equilibrated with 1 column volume (CV) of wash buffer--Buffer A (300 mM NaCl, 50 mM Tris, pH 8.0). The flow rate was maintained at 5 mL/min. Unbound proteins were removed by flushing the column with 10 CVs of elution buffer--Buffer B (300 mM NaCl, 50 mM Tris, 500 mM Imidazole, pH 8.0) at the same flow rate. The His-tagged MRSaFBA proteins were then eluted using a linear gradient of 0-100% imidazole.

2.1.3. Secondary Purification and Final Protein Yield

To achieve a relatively pure MRSaFBA protein, a series of four purification steps were implemented. The MRSaFBA protein, tagged with a His-tag, initially underwent purification using Immobilized Metal Affinity Chromatography (IMAC). The procedure involved loading the filtered MRSaFBA solution onto a 5 mL HisTrap FF IMAC fast flow column, pre- equilibrated with 1 column volume (CV) of equilibration and wash buffer-- Buffer A (300 mM NaCl, 50 mM Tris, pH 8.0). The flow rate was maintained at 5 mL/min. Unbound proteins were removed by washing the column with
10 CVs of elution buffer--Buffer B (300 mM NaCl, 50 mM Tris, 500 mM Imidazole, pH 8.0) at the same flow rate. Elution of His-tagged MRSaFBA proteins was achieved through a linear gradient of 0-100% imidazole.

Post-elution with 500 mM imidazole, the chromatographic peaks were analyzed via SDS-PAGE. Fractions displaying distinct bands around 33 kDa, yet containing significant impurities, were deemed insufficiently pure for subsequent gel filtration. Consequently, a second IMAC purification was scheduled, employing a modified imidazole gradient to remove impurities while preserving the majority of the MRSaFBA protein.

To prepare for the second IMAC step, the protein sample underwent desalting to exchange the imidazole-containing buffer with Buffer A. This was accomplished using an EPPF-Desalting 26/10 column (GE Healthcare, USA), equilibrated with Buffer A at a flow rate of 5 mL/min until a stable baseline was observed. The protein sample was loaded onto the column at 1 mL/min. Desalted proteins were collected in the flow-through, while salts and smaller molecules were retained within the column matrix. Protein elution was monitored at 280 nm, and fractions were pooled based on chromatogram peaks.

Following desalting and buffer exchange, a second IMAC purification was conducted. The elution was performed with sequential holds at 10%, 60%, and 100% Buffer B. This process yielded two peaks, with the second peak containing relatively pure MRSaFBA protein. Final purification via gel filtration resulted in a protein concentration of 0.5 mg/mL.

2.1.4. Gel Filtration of the First Batch of Protein

A total of 4.5 mL of protein sample, which had undergone three prior purification steps, was subjected to gel filtration using a HiPrep 16/60 Sephacryl S200 HR column (120 mL). The column was equilibrated with the same purification buffer used in the IMAC step. The gel filtration was carried out at a flow rate of 0.5 mL/min. Following gel filtration, two distinct peaks were observed in the chromatogram. Fractions corresponding to these

peaks were analyzed via SDS-PAGE, and the relevant fractions containing FBA were pooled.

The concentration of the samples after the four-step purification process was determined by measuring absorbance at 280 nm (A280) using an extinction coefficient of insert specific extinction coefficient value $M^{-1} \cdot cm^{-1}$. The resulting concentrations were 1.18 mg/mL for the first peak and 1.20 mg/mL for the second peak. These fractions were then divided into 0.2 mL aliquots, flash-frozen in liquid nitrogen, and stored at -80°C. These samples were designated as MRSaFBA first peak and MRSaFBA second peak, respectively.

2.1.5. Batch-2: Production and Purification

The overall production and purification process for Batch-2 was largely consistent with Batch-1, with two significant modifications. Instead of mechanical disruption, enzymatic lysis was employed using BugBuster Master Mix (Novagen, Cat. No. 71456, Lot N47647-2).

In Batch-1, the first IMAC did not perform as effectively as anticipated, necessitating a more extensive purification process. Specifically, two IMAC steps and one desalting process were required before the sample could proceed to gel filtration. This multi-step purification was essential to achieve a sufficient level of purity, as the initial IMAC did not adequately remove impurities, necessitating additional steps to enhance the quality of the protein sample.

For Batch-2, informed by the challenges encountered in Batch-1 and particularly the elution patterns observed during the second IMAC, the purification process was streamlined. Step elution was implemented, starting with 5% Buffer B and then proceeding directly to 100% Buffer B. The fraction with the highest concentration was immediately subjected to gel filtration using a HiPrep 16/60 Sephacryl S300 HR column. This optimized approach reduced the purification timeline significantly, decreasing the time from initiation to gel filtration from two weeks (as observed in Batch-1) to just two days.

For samples that underwent the three-step purification but were not subjected to gel filtration, SDS-PAGE analysis was performed to assess their purity. Relatively pure samples, exhibiting a strong band at approximately 32 kDa, were collected. The total volume of the protein sample before proceeding to the gel filtration step was 15 mL.

2.2. Characteristics

2.2.1. Dynamic Light Scattering (DLS) Analysis of MRSaFBA

Dynamic Light Scattering (DLS) was utilized to determine the particle size distribution, hydrodynamic radius (rH), and polydispersity index (PDI) of MRSaFBA, reflecting the homogeneity or heterogeneity of particle sizes within the sample. The DLS technique involves passing a laser beam through the sample and monitoring the scattered photons at specific angles over microsecond intervals, which are influenced by the relative positions of particles in the solution.

Three experiments were conducted to evaluate the physical properties of MRSaFBA samples using DLS: (1) freshly purified protein from the first batch, (2) protein from the first batch after one month of storage at 4°C, and (3) freshly purified protein from the second batch. These experiments aimed to assess the hydrodynamic radius (rH) and polydispersity index (PDI) of the protein, providing insights into the various forms present and how these forms may change over time or with different purification methods. This information is crucial for ensuring the quality and reliability of the protein used in subsequent experiments. In enzyme assays, in particular, the physical state of the protein can significantly impact the results, making it essential to thoroughly understand and control these variables.

The analysis was performed using a Zetasizer Auto Plate Sampler (Malvern Instruments) equipped with a 4 mW He-Ne laser (λ = 633 nm, θ = 173°). Prior to analysis, the MRSaFBA samples were gently thawed on ice and prepared at a final concentration of 1

mg/mL in aqueous solution. Both the samples and the buffer were filtered through a 0.45 μm filter to remove any aggregates or dust particles. Additionally, the MRSaFBA samples had been centrifuged using a JA25.50 rotor at 13,000 rpm for 20 minutes to further ensure sample purity.

Measurements were conducted using a 96-well plate, with 60 μL of MRSaFBA samples loaded into each well, along with buffer controls. All samples were maintained at room temperature during the analysis.

2.2.2. Thermal Denaturation Analysis (TDA) of MRSaFBA

Thermal Denaturation Analysis (TDA) was utilized to evaluate the thermal stability of MRSaFBA by measuring the unfolding temperature transition, known as the melting temperature (Tm). This assay allows for the identification of conditions that significantly change Tm by altering solution conditions and adding various stabilizing agents. Additionally, observing modification of Tm upon ligand binding enables the use of TDA as a low-cost preliminary screening method for discovering new protein- ligand interactions [79].

As the temperature increases during the assay, proteins begin to unfold, exposing hydrophobic regions to which the Sypro Orange reagent binds, resulting in a measurable increase in fluorescence emission (490-580 nm).

For the TDA, the Biometra TOptical rtPCR system was employed. Samples were prepared in triplicate, with a final volume of 200 μL per sample under varying conditions, and 50 μL of each sample was injected per well. Each sample contained 10x SYPRO Orange dye and 6 μM MRSaFBA in Gel Filtration (GF) Buffer (50 mM TEA, 100 mM KCl, 10 mM $MgCl_2$, 10% glycerol, pH 7.2), with or without ligands or metal ions.

The samples (50 μL each) were placed in a 96-well PCR plate (BioRad), which was then rotated at 1000 rpm at 4°C for 5 minutes. The plate was sealed with tape (BioRad), and the assay parameters were set, with the temperature ramping from 25°C to 74.5°C. Fluorescence changes were monitored at 0.5°C intervals, and measurements were initiated to track the thermal denaturation process.

2.2.3. Enzyme Assay

All enzyme assays were conducted in triplicate using 96-well plates at 25°C, with absorbance readings at 340 nm recorded over time. The enzymatic activity of MRSaFBA was assessed indirectly by measuring the decrease in absorbance of reduced nicotinamide adenine dinucleotide (NADH) at 340 nm using a SpectraMax M5 96-well multimode microplate reader. The activity of MRSaFBA was evaluated by monitoring the reduction of NADH in the presence of the substrate fructose 1,6-bisphosphate.

In this assay, MRSaFBA catalyzed the conversion of fructose 1,6- bisphosphate into dihydroxyacetone phosphate and glyceraldehyde-3- phosphate. The glyceraldehyde-3-phosphate was then completely converted to dihydroxyacetone phosphate by the addition of excess triosephosphate isomerase (TIM). Subsequently, dihydroxyacetone phosphate was converted to glycerol-3-phosphate by excess glycerol-3- phosphate dehydrogenase, with the concurrent consumption of 2 moles of NADH per mole of fructose 1,6-bisphosphate. The oxidation of NADH was monitored at a wavelength of 340 nm, with a stoichiometric ratio of 1:2 for NADH consumption relative to fructose 1,6-bisphosphate.

To convert the change in absorbance at 340 nm (A340) to enzymatic activity rates, a nearly linear segment was selected from the time- absorbance plot. The rate of change in absorbance per second was calculated from this interval and then multiplied by 60 to convert it into a per-minute rate.

Subsequently, the Lambert-Beer law was applied, where AU represents the absorbance, and the molar absorptivity of NADH at 280 nm, was given as 6220 $M^{-1} \cdot cm^{-1}$. The concentration of the solute (in mol/L) was derived, resulting in the determination of the change in NADH molarity per minute.

This value was then converted to the number of moles of NADH converted per minute in a 1 mL reaction volume, considering a stoichiometric ratio of 1:2 for NADH consumption relative to fructose 1,6- bisphosphate. By dividing the change in molarity of NADH per minute by 2000 (1000 for mL to L conversion and 2 for the stoichiometric ratio), the rate of NADH turnover in $mol \cdot min^{-1}$ was obtained, which was then scaled to $\mu mol \cdot min^{-1}$ by multiplying by 1,000,000.

Finally, this turnover rate was normalized to the protein amount in the 100 µL reaction mixture. The working concentration of the protein in the enzyme activity experiment, set at 7 µM (7×10^{-6} M), was multiplied by the theoretical molecular weight of the monomeric unit (32.56 kDa) and the volume (0.1 mL), and converted to mg. The result, the specific enzyme activity, was expressed in $\mu mol \cdot min^{-1} \cdot mg^{-1}$, providing a detailed quantification of the enzyme's catalytic capabilities under the specified experimental conditions.

2.2.4. Model Building and Molecular Docking

(a) Sequence Alignment: To model the binding of the inhibitor HCA to the MRSaFBA protein, the MtFBA protein structure (PDB ID: 4LV4) was used as a reference, given that it has HCA bound within its active site. The sequence of MRSaFBA (PDB ID: 4TO8) was aligned with that of 4LV4 using two modelling methods: Swiss-Model and Phyre2.

Swiss-Model [56,72] facilitates protein structure prediction by automatically identifying homologous templates from the Protein Data Bank (PDB) and then using sequence alignment to map the target sequence onto the template, thereby generating a model through comparative protein modelling. Phyre2 employs a combination of hidden Markov models and advanced heuristics to scan against a database of known protein structures, aligning the target sequence to the most compatible templates to predict and build a three-dimensional structure with high confidence.

The alignment focused on structural similarities and differences within the active site to ensure accurate accommodation of HCA. In the 4LV4 structure, His96 forms a Pi-sulfur interaction with Met129 and hydrogen bonds with aspartic acids and glutamic acid residues, serving as key points of comparison for the MRSaFBA alignment.

(b) Structural Alignment: Following the sequence alignment, the MtFBA protein structure (PDB ID: 4LV4) was used as a template to adapt the MRSaFBA protein (PDB ID: 4TO8) for HCA binding. Initial sequence alignment using Swiss-Model and Phyre2 integrated the MRSaFBA sequence with the 4LV4 structure, but the resulting models did not align well with the active site of 4LV4.

To address this, further refinement was performed by superimposing chain A of 4TO8 onto 4LV4 using PyMOL. Structural refinement was subsequently conducted using Coot, Phyre2, and manual adjustments to correct sidechains and integrate the zinc ion critical for HCA binding.

Final structural alignment and molecular docking simulations were carried out using LeDock, which resulted in a root mean square deviation (RMSD) of 0.246 for 164 atoms when compared to the 4LV4 structure, indicating a high degree of alignment accuracy. It is important to note that the final structural model of the MRSaFBA protein used for docking was constructed by Dr. Iain McNae.

3. Results

3.1. Production and Purification of MRSaFBA

3.1.1. First Batch of Protein

The first IMAC purification step (shown in Figure 1) utilised an imidazole gradient from 0 – 500 mM over 10 column volumes. A single broad peak can be seen in the elution section of the chromatograph, but the purity of FBA across the latter half of the peak is poor (≤ 70%). Even though the yield of FBNS is high (sate what it is), the purity is not good enough for further work/assays.

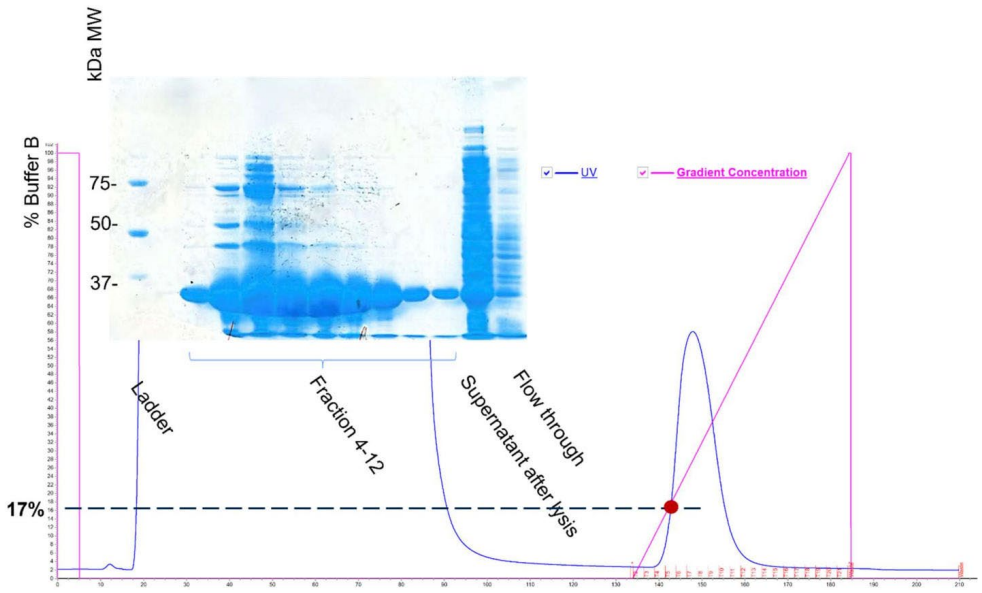

Figure 1. Purification of MRSaFBA: IMAC. Elution profile of MRSaFBA from 5 ml HiTrap IMAC column and imidazole linear gradient method to elute. Fractions from elution (4-11) were pooled. Analysis of fractions in 12% acrylamide SDS-PAGE Coomassie stained gel.

The strategy involved adjusting the concentration of Buffer B to effectively separate MRSaFBA from various other proteins present in the cell lysate, including enzymes, structural proteins, and other cellular components, as well as nucleic acids, lipids, and cell membrane fragments. Additionally, potential contaminants such as endotoxins, including lipopolysaccharides from the bacterial outer membrane, needed to be removed to achieve the purification of the target protein. The precise concentration of Buffer B required to elute MRSaFBA was initially unknown. Therefore, a stepwise elution strategy was employed, beginning with a 10% Buffer B hold, followed by a 60% Buffer B hold, and finally a 100% Buffer B elution. As depicted in Figure 2, two distinct peaks were observed. The second peak was deemed sufficiently pure and was subsequently subjected to gel filtration for further purification.

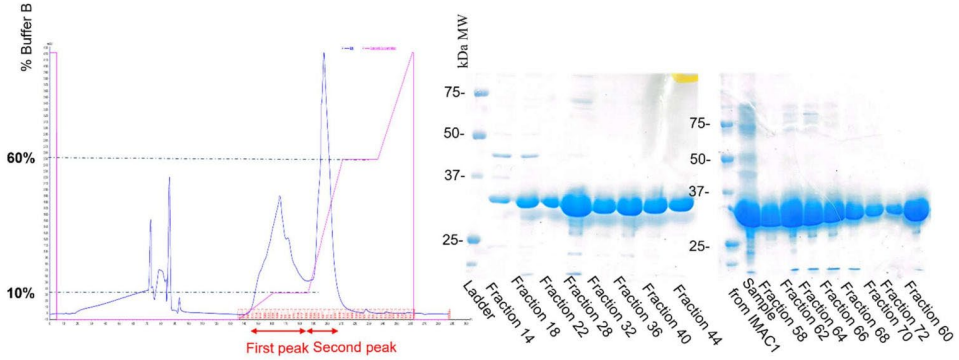

Figure 2. Purification of MRSaFBA: Second IMAC. Elution profile of MRSaFBA from 5 ml HiTrap IMAC column and imidazole gradient method of climbing to 10% in 5CV, hold for 5CV, then climb to 60%, hold for 5CV, finally climb to 100% to elute. Fractions from elution (36-44, 58-69) were pooled; Analysis of fractions in 12% SDS-PAGE Coomassie stained gel.

From the manufacturers supplied calibration curve, the elution positions of 46 mL and 61 mL correspond to apparent molecular weights of 75 kDa and 43 kDa according to Gel Filtration Calibration Kit LMW Manufacture. These are consistent with theoretical weights of monomeric and dimeric FBA (32.56 kDa and 65.12 kDa, respectively). As the known active form of MRSaFBA is dimer [80], the second peak was expected to be MRSaFBA that was wanted. Taken both peaks in to SDS-PAGE (Figure 3), it was showed on the gel that both two peaks contained components with a molecular weight corresponding to the monomeric form of MRSaFBA (32.56 kDa). However, samples from the first peak also contained other lower molecular weight substances, indicating impurity. Therefore, the second peak was selected for further study. The proteins obtained from the second peak were pooled together to obtain a sample with a concentration of 0.5 mg/ml, which was then concentrated to 1.1 mg/ml and stored frozen.

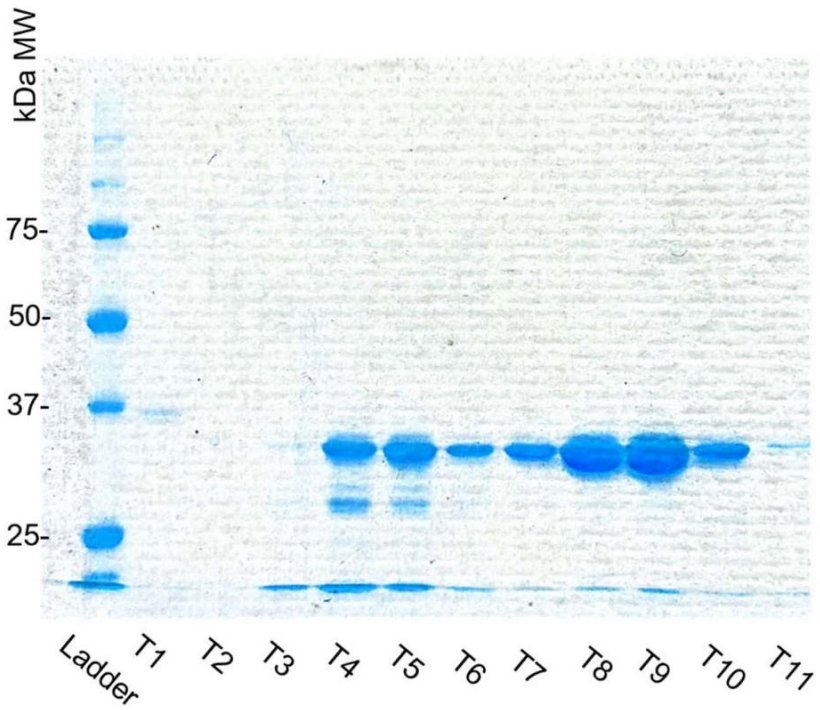

Figure 3. 12% SDS-PAGE Coomassie stained gel of sample fractions post- Gel filtration: MW: molecular weight marker; Fractions from 1 to 11 that contain MRSaFBA, where T1-T6 came from the first peak, T7-T11 came from the second peak.

3.1.2. Second batch of protein

The second time of purification and expression, instead of Mechanical Disruption, Enzymatic Lysis was used. Then, learnt from the first time of purification and expression process, and analyzed the figure from the second IMAC carried out in the first time, it was informed of when MRSaFBA mainly came off, so here the setting was changed to step elution, starting at 5% and straight to 100% Buffer B, then the peak with highest concentration go straight to gel filtration process. During the second time of purification, the whole process only took two days for the protein sample to get on to gel filtration column, without staying in high concentration of imidazole two weeks longer. When looking into the SDS-PAGE result of this time, main binds appeared at around 33kDa for both two peaks, the same MW as monomer form of MRSaFBA (it should be noted that SDS-PAGE was done after putting sample on s300 column as the idea was to keep the process as fast as possible); there were still smaller impurities in the first peak. For gel filtration result of this time, still two peaks were obtained, and they came off at similar retention volume. However, when pulled the samples from second peak together, a concentration of

0.8mg/ml was obtained, which was higher than former one. As the volume that went into gel filtration column was the same, the amount of protein gained this time was about 1.6 times more than the former batch of protein.

3.1.3. Conclusion and comparison between first and second batch of protein

The amount of the proteins obtained from the first purification differed significantly from the published Km values for MRSaFBA substrates. This observation suggested that improvements could be made in the purification process. The two mentioned changes—switching to enzymatic lysis and minimizing the time proteins spent in high imidazole concentrations—could potentially impact protein stability and thereby improve the final enzyme activity and consistency.

In comparing the two purification processes, aside from the adjustment in imidazole elution concentration during IMAC to reduce protein loss, there are several other differences: Lysis Method modification, in the second batch, enzymatic lysis was used instead of mechanical disruption, which was employed in the first batch. It was in accordance with what Capodagli et al. did by lysing protein with chicken lysozyme followed by sonication [80]. Despite of the fact of higher cost, enzymatic lysis offers a gentler alternative to mechanical disruption for cell lysis, preserving the integrity and functionality of sensitive proteins [81]. It results in higher yields of active proteins with reduced cellular debris and is particularly beneficial for maintaining protein structure, which is in accordance with the result in DLS and enzyme assay when comparing the two batch of protein; moreover, for imidazole exposure, during the second purification, the protein was not exposed to high concentrations of imidazole for an extended period. When comparing and analysing the purification process, it was suspected that it was possible that high concentrations of imidazole could have an effect on the stability of the proteins, as Imidazole has a strong coordination ability and can form complexes with metal ions [82], whereas for metal element- dependent MRSaFBA this may indeed have an effect on its stability.

3.2. Characteristics

3.2.1. DLS

Two groups of experiments were conducted to compare and analyze MRSaFBA under different storage times and purification methods. The results are illustrated in the following Figure 4. These comparisons provide insights into the effects of storage duration and purification techniques on the protein's properties as measured by Dynamic Light Scattering (DLS).

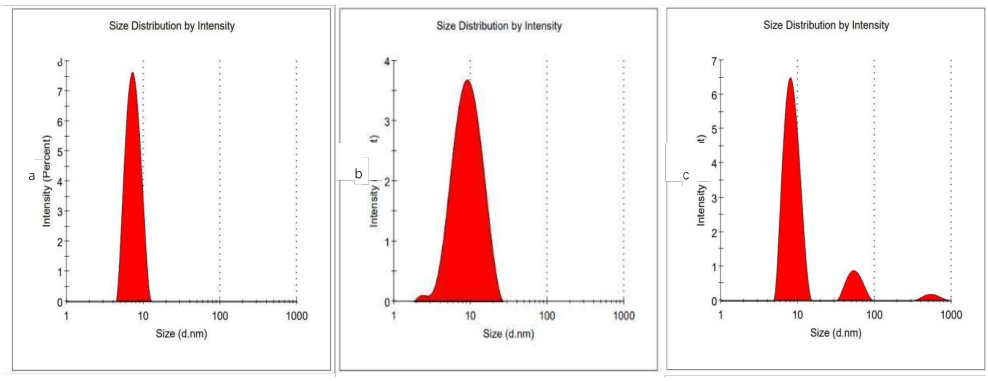

Figure 4. DLS Analysis of MRSaFBA: Effects of Purification and Storage Conditions, (a) represents the MRSaFBA protein obtained from the first purification, (b) shows the MRSaFBA protein obtained from the first purification but frozen for one month. (c) depicts the MRSaFBA protein obtained from the second purification.

As is shown in Figure 4, Panel a displayed a sharp, narrowly peaked distribution centered around a small diameter, indicating that the majority of the MRSaFBA protein was predominantly monodisperse immediately following the first purification. The sharp peak suggested that the sizes of the majority of the protein particles were uniform, typically indicative of good purification with relatively minimal aggregation; Panel b showed a peak that was broader than that in Panel a, indicating an increase in polydispersity. This broadening could be interpreted as the protein having undergone some level of aggregation or having formed multiple particle sizes over time; Panel c suggested the presence of various aggregated forms or possibly oligomeric states of the protein. It was indicative of ongoing degradation or fragmentation, showing multiple peaks, including one significantly larger than those observed in Panels a and b.

(I)Analysis of DLS Results for MRSaFBA under Different Storage Times and Purification Methods

The dynamic light scattering (DLS) results for MRSaFBA reveal significant changes in stability under different storage times and purification methods [83]. Over time, the protein exhibits a broader peak and an increased average particle size, suggesting a more relaxed and less dense structure compared to fresh protein. This results in the presence of various protein states. Additionally, the appearance of a small low-molecular-weight peak may indicate degraded protein fragments. When comparing protein concentrations after one month, increases in rH (average particle size) and SD (standard deviation) indicate greater polydispersity and aggregation, suggesting instability, potential denaturation, or structural changes [84]. The reported monomer molecular weight of the protein is about 32 kDa, and its existing active form dimer is about 64 kDa. Freshly purified protein has an estimated molecular weight of 58.9 kDa, while stored protein shows a molecular weight of 43.7 kDa, indicating degradation over time. This significant reduction suggests ongoing degradation or fragmentation. The discrepancy between the reported molecular weight and that of the freshly purified protein may be due to post-translational modifications or incomplete removal of tags or other associated molecules during purification.

A new purification method using lysozyme instead of ultrasonic disruption was employed. Ultrasonic disruption uses high-frequency sound waves to break cell walls and membranes through mechanical shear forces, vibrations, and localized heating [85]. This method is efficient but requires cooling to prevent protein denaturation. Conversely, lysozyme lysis hydrolyzes polysaccharides in bacterial cell walls, making it effective primarily for Gram-positive bacteria [86]. It is a gentler process that protects proteins and nucleic acids, though it is less efficient and limited to specific cells. Chemical disruption, being gentler, is less likely to damage the target protein but may result in incomplete bacterial lysis. Mechanical disruption, being more intense, can damage protein structures if power is not controlled well, leading to precipitation and lower yield. DLS results can reveal structural damage to the protein. Protein obtained by mechanical methods shows a single peak below 10, while protein obtained by chemical disruption shows multiple high-molecular-weight peaks, indicating the formation of oligomers [87]. To study whether these oligomers are a normal physiological phenomenon, further experiments are needed to compare the oligomeric state of the protein in different conditions and environments. In the following enzyme activity assay, when comparing these two batches of protein purified by different way (Figure 5), it shows that former batch of protein was about 18% less active than newly produced protein using modified purification process.

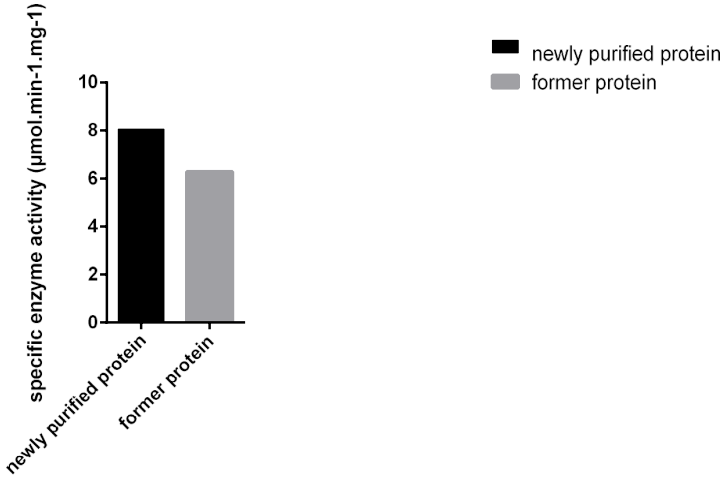

Figure 5. Comparison of Specific Enzyme Activity Between Newly Purified using Modified Purification Process and Former Protein Samples, both under the condition of 7 μM of MRSaFBA and 0.5 mM of FBP to start the reaction.

(II)Impact of Glycerol on DLS Measurements and Protein Hydrodynamic Radius

In dynamic light scattering (DLS) measurements, the presence of 5% glycerol in the buffer significantly affects the results, often resulting in the appearance of larger peaks that do not belong to proteins [88]. This may be due to the fact that glycerol itself can form small aggregates or droplets in solution, which may be detected as particles by DLS. These glycerol aggregates can show spikes in the size distribution that are larger than the actual protein particles, and in MRSaFBA's DLS results, whether newly made protein, stored protein, or the second batch of protein derived from the new method, The MW peak was larger than protein itself, and the presence of glycerol is likely to be the cause of this peak. In addition, glycerol will increase the viscosity of the buffer, which will affect the scattering intensity and diffusion behavior of the particles. Higher viscosity slows the Brownian motion of the particles and may alter the apparent hydrodynamic radius (Rh) measured by DLS. Compared with the value of 8.3 nm obtained by taking the maximum radius in pymol, the rH measured by DLS is about 9.238 nm, which is slightly larger than that observed in pymol, which may also be influenced by glycerol. Therefore, to minimize the influence of glycerol on DLS measurement, a control experiment was conducted using buffer solution (without protein) alone to determine the corresponding peak of glycerol aggregates. This helps to distinguish peaks from buffers and peaks from protein samples.

3.2.2. TDA

(a) Effects of Zinc Concentration on the Thermal Stability of MRSaFBA: Destabilization at Low and Stabilization at High Concentrations

Zinc destabilized MRSaFBA under low concentration while stabilized it under relatively high concentration The horizontal coordinate was the point measured and recorded every 0.5 degree from 25 degrees to 74.5 degrees; The ordinate was relative fluorescence units (RFU), which was used to assess the presence and concentration of fluorescent molecules in a sample.

The melting temperature of protein only group under 6μM concentration was 62.5°C. After adding 1uM 10uM, 50uM, 100uM of relatively low concentration of zinc, the melting temperature decreased, indicating certain degree of destabilization; while for 1Mm, 5mM of zinc, showing a shift to higher melting temperature, indicating stabilization. However, such high concentrations of zinc are not physiologically relevant. Therefore, even if zinc at these concentrations can make the protein more stable, high concentrations of zinc should not be used in subsequent enzyme assay experiments. This topic will be discussed in detail in the result and discussion section of the enzyme assay.

(b) Investigating the destabilizing effects of HCA on MRSaFBA and giving potential mechanisms and structural Implications

Concentrations of HCA, under the same condition of 6 μM MRSaFBA, 10 μM of zinc)

HCA is a known inhibitor for MRSaFBA, without published pdb structure containing HCA in its structure. However, when putting 1mM of HCA into enzyme assay system (with 6μM of MRSaFBA, 10μM Zncl2, with a SD value of 0.01), it indicated a decrease in melting temperature, from 52°C to 45.5°C. This suggested that HCA destabilize MRSaFBA. Destabilization in TDA can be caused by multiple reasons, combining the fact that HCA was shown to have effect on MRSaFBA on the enzyme assay as well as the fact that it's a known inhibitor of MRSaFBA, three possible hypothesis was raised.

Firstly, HCA working as chaotropic agent. When screening for potential inhibitors or activators through TDA (thermal denaturation assays), it is common to select ligands that bind to the protein and stabilize it. This is because ligands that cause destabilization do not necessarily indicate binding at the active site; they could be functioning as chaotropic agents. Chaotropic agents are compounds that disrupt the hydrogen bonding network within proteins, leading to denaturation and loss of secondary and tertiary structure. They exert their effects by interfering with the non- covalent interactions that stabilize protein structure, such as hydrogen bonds, hydrophobic interactions, and van der Waals forces. As a result, chaotropic agents can cause proteins to unfold or aggregate, impacting their function. Enzyme inhibition kinetics show that HCA binds to allosteric sites, indirectly affecting the active cavity through the protein's hydrogen- bond network, impacting substrate metabolism [89]. This may influence substrate binding, metal ion complexation, and the spatial structure of active amino acid sites [88].

Another possibility is that HCA can function as a metal chelator.

However, HCA is unlikely to act as a metal ion chelator due to the absence of necessary functional groups, such as hydroxyls, carboxylates, or amines, which are typically involved in coordinating metal ions (Figure 6). Consequently, HCA cannot form stable chelates with metal ions, limiting its potential as a metal ion chelator.

Figure 6. 3D Model of a Quinolone Antibacterial Agent, 8-.

hydroxyquinoline carboxylic acid (HCA), which depicts a molecular structure, rendered in a 3D model format. It features a molecule consisting of two benzene rings, with one of the rings containing a nitrogen atom (highlighted in blue).

Moreover, while HCA binds to the active site, it destabilizes the protein's structure, potentially through mechanisms akin to those of chaotropic agents, by disrupting key interactions and altering the spatial configuration of active site residues. Since the published PDB structure of MRSaFBA-HCA is not available, we refer to the impact of HCA on MtFBA as a reference [82]. The 2.1 Å X-ray crystal structure shows that HCA coordinates with Zn(II), displacing His212 and Val165, and forms a hydrophobic pocket. This interaction results in the loss of key structural elements around the active site, blocking substrate access. These interactions result in significant alterations to the active site structure of MtFBA. If HCA similarly affects the structure of MRSaFBA upon binding, this structural disruption could be one of the reasons for the observed instability of MRSaFBA in the presence of HCA.

(c) Compare old/new under 6uM concentration of protein, new one(51°C) is slightly less stable than the old one (53°C)

From Figure 7, when comparing the melting temperatures of the protein obtained from the second fresh purification at the same concentration than the protein obtained from the first and left for a month and a half. The stability of the second freshly purified protein (Tm = 51°C) was slightly lower than that of the first obtained (Tm = 53°C).

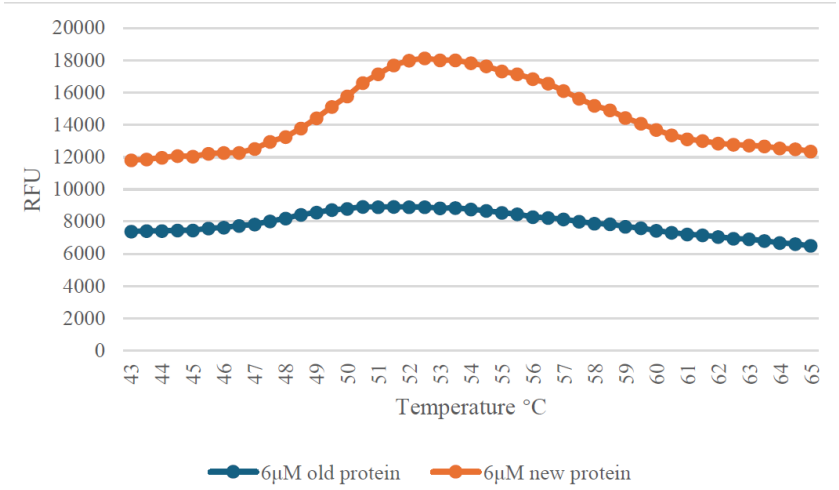

Figure 7. Comparison of Thermal Stability Between Old and New Protein Batches under 6 μM of MRSaFBA.

The melting temperature (Tm) is an indicator of protein stability in thermal denaturation assays. Tm is the temperature at which 50% of the protein is unfolded or denatured. The higher the melting temperature indicates a more stable protein, as it tends to require a higher temperature to reach 50% denaturation of the molecule, suggesting a stronger or more stabilised interactions in its structure [90,91].

From my result, under a 6 μM of both batch of protein concentration, the newly purified protein (Tm = 51°C) was slightly less stable compared to the former batch of protein (Tm = 53°C). Comparing the modification in the purification process between these two batches of protein, the different Tm may be a result of the presence of imidazole. According to the purification section, the first batch of protein was left in the high concentration of imidazole about two weeks longer than the new batch. The presence of imidazole can significantly affect protein stability through various mechanisms. Electrostatic interactions with charged solvent molecules at the protein surface contribute to the stability of the protein [92]. Electrostatic interactions with charged solvent molecules at the protein surface contribute to stability [91]. Imidazole, with its strong coordination ability, can form complexes with metal ions, potentially affecting structural integrity.

3.2.3. Enzyme Activity

(a) The effect of zinc on enzyme activity; and comprehensive analysis of zinc's potential impact on MRSaFBA: TDA and Enzyme Activity Conclusions

In class II FBAs (Fructose-bisphosphate Aldolases), the reaction mechanism utilizes Zn(II) cations as a catalyst to stabilize the enediolate intermediate of DHAP, thereby efficiently facilitating the aldol condensation reaction. The presence of zinc is crucial for the enzymatic catalytic activity of class II FBAs. Moreover, referencing the reaction mechanism of MtFBAHCA, it appears that HCA exploits the previously overlooked sensitivity of MtFBA's His212 to Zn(II) coordination and the structural dependency of this interaction on the Z-loop. MtFBA apo structure of Santangelo et al. indicates that the ordered structure of the Z ring is dependent on the presence of Zn(II) within the active site [93]. Capodagli et al. [80] discover that the Fo-Fc density of citrate molecules is coordinated with the active site Zn(II) in a tridentate manner. This interaction is remarkably similar to the previously observed interaction between MtFBA and the Z- loop inhibitor HCA. As shown

in Figure 8 (b) and Figure 9 (a), when constructing models, the binding site from MtFBA-HCA was used as a reference to modify the structure of MRSaFBA. This consideration includes examining the role of zinc in the MRSaFBA-HCA interaction and the potential involvement of possible binding ligands in influencing these interactions.

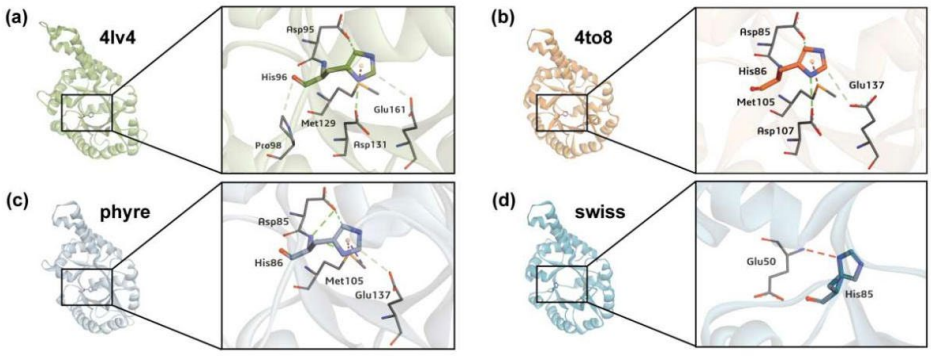

Figure 8. 3D Interaction Analysis of the Proton Acceptor in Different Protein Structures: (a) 4LV4: Visualization of the proton acceptor interactions in the MtFBA protein structure, where His96 acts as the proton acceptor. (b) 4TO8: Interaction analysis of the proton acceptor in the MRSaFBA protein structure, with His86 acting as the proton acceptor. (c) Phyre Model: Proton acceptor interactions in the Phyre model, where His86 (corresponding to His96 in 4LV4) acts as the proton acceptor. (d) Swiss-Model: Proton acceptor interactions in the Swiss-Model, where His85 (equivalent to His96 in 4LV4) acts as the proton acceptor but is misaligned compared to the other structures. The color in the small molecules indicate different atoms: carbon (matching the color of the protein structure), oxygen (red), nitrogen (blue), and sulfur (yellow). Color coding of interactions: green lines represent hydrogen bonds, pink lines indicate hydrophobic interactions, orange lines denote electrostatic interactions, and purple lines show π-π stacking interactions.

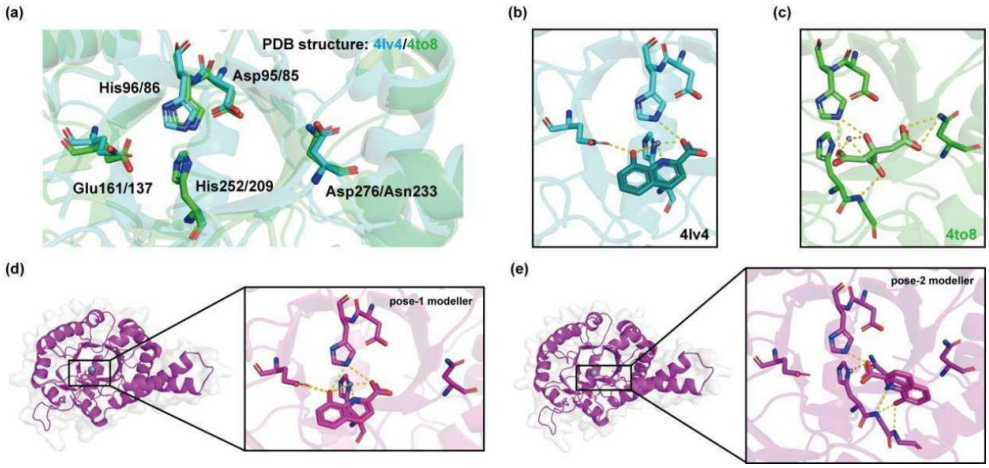

Figure 9. Comparative 3D Interaction Analysis of the Active Sites: (a) Overview of the active sites of PDB structures 4LV4 and 4TO8. Structural differences and alignment issues are highlighted, demonstrating the incompatibility of 4TO8 with HCA. (b) 3D protein-ligand interaction analysis of HCA bound to the active site of 4LV4. Key interactions include polar bonds formed by Glu161, His96, and His252 with the ligand. (c) 3D protein-ligand interaction analysis of FLC bound to the active site of 4TO8. Key interactions involve His86, His209, and Asn233 with the ligand. (d) 3D protein-ligand interaction analysis of HCA pose 1 bound to the active site of the model. This pose closely replicates the binding mode of HCA in the 4LV4 structure, indicating an accurate reproduction of the ligand's interactions. (e) 3D protein-ligand interaction analysis of HCA pose 2 bound to the active site of the model. This pose shows alternative binding interactions, including additional hydrogen bonding with Gly210 through the hydroxyl group. Colors represent different atoms: carbon (grey), oxygen (red), nitrogen (blue), and sulfur (yellow). Yellow lines indicate hydrogen bonds.

Acknowledgement: The structural model of the MRSaFBA protein was constructed by Dr. Iain McNae.

Therefore, a zinc gradient assay was conducted. The results showed that zinc at relatively low concentrations activated MRSaFBA, while higher concentrations led to inhibition. Specifically, at 5 μM and 10 μM zinc, the specific enzyme activity increased by 24 ± 4% and 16 ± 6%, respectively, compared to the protein-only group. In contrast, at 100 μM, 0.5 mM, and 1 mM zinc, enzyme activity was inhibited by 86 ± 2%, 96 ± 3%, and 98 ± 2%, respectively.

Combine with the conclusion from TDA result that Tm of relatively low concentration of zinc, the melting temperature decreased, indicating certain degree of destabilization; while for relatively high concentration of zinc, it showed a shift to higher melting temperature, indicating stabilization.

This gives an idea that structural wise stabilization does not necessarily mean better activity, and when designing experiments, it's important to consider biological relevance.

After examining the effects of both low and high zinc concentrations on MRSaFBA, contrasting with previous research that focused mainly on high concentrations [80,89]. Low zinc levels enhance MRSaFBA's activity and stability, while high concentrations may occupy the active site, reducing substrate binding and protein degradation. Effective zinc concentration control is essential for maintaining MRSaFBA's functionality and stability. MRSaFBA exhibits activity in the presence of small amounts of zinc ions, indicating it is a metal-ion-dependent protein [94,95]. Activated protease activity in the presence of zinc ions may lead to self-digestion and protein degradation [96]. In such cases, it is recommended to reduce the storage concentration of the protein. Zinc ions can also transform the protein from an inactive state to an active receptor state, making the protein more sensitive to external energy changes, resulting in decreased thermal stability. In high concentrations, zinc ions competitively occupy the active site of the protease, preventing substrate access, thus stabilizing the protein. High concentrations of metal ions may also interact with the protein's hydration surface, slowing down denaturation and aggregation [97,98].

Additionally, when studying HCA's inhibition ability against FBA, Capodagli et al. [80] conduct experiments under the condition of excess of zinc, however, in the presence of excess zinc, the reversible inhibition mechanism may present false positives, as zinc blocks HCA's ability to bind to the active site, showing only non-competitive inhibition [99].

(b) From Figure 5, it shows that after one month of storage, when comparing these two batches of protein purified by different ways, former batch of protein was 18% less active than newly produced protein using modified purification

When comparing the proteins purified by two different methods, the second batch obtained through a modified purification process suggested the presence of protein oligomers, potentially indicating aggregation. In enzyme activity assays, the second batch of protein was found to be 18% more active than the first batch. The formation of these oligomers could be a result of structural damage or protein aggregation.

However, despite the potential for protein oligomerization, the observed enzyme activity suggests that these oligomers might represent the normal physiological state or functional assembly of the protein in vivo. This hypothesis is supported by the fact that certain proteins naturally exist as oligomers under physiological conditions, where they play crucial roles in their biological functions. To further explore this hypothesis, in vivo studies could be conducted to compare the oligomeric state of the protein under different conditions and environments. Such studies would help determine whether the observed oligomers are functional and biologically relevant. To elucidate the functional significance of different oligomeric states of proteins under varying conditions, in vivo studies can be conducted using genetically engineered mouse models. Employing techniques such as Bioluminescence Resonance Energy Transfer (BRET) and Fluorescence Resonance Energy

Transfer (FRET), as referenced in Chen et al., will allow real-time monitoring of protein interactions and oligomerization [56]. Functional relevance will be assessed through behavioral and physiological tests, influenced by environmental factors such as temperature changes and chemical treatments.

3.2.4. Model Building and Molecular Docking

1) Models built from structure alignment

In the process of investigating the structural modifications required for the protein MRSaFBA (PDB ID: 4TO8) to accommodate the small molecule inhibitor HCA, which is known to inhibit 4TO8 but is not present in its PDB sequence, an essential reference structure is the MtFBA protein (PDB ID:
4LV4). The 4LV4 structure already has HCA bound at its active site, providing a critical benchmark for the modifications needed in 4TO8. Two modelling methods were employed: Swiss-Model, and phyre model. As shown in Figure 10a, each generated model was then compared to the 4LV4 structure, particularly focusing on the active site, to identify structural similarities, differences, and alignment issues.

In the 4LV4 structure (Figure 10b), His96 acts as a proton acceptor and forms a Pi-sulfur interaction with the nearby Methionine at position 129 (Met129). Additionally, His96 engages in hydrogen bonding with two aspartic acids (Asp) and one glutamic acid (Glu) side chains, which are negatively charged. In the 4TO8 structure (Figure 10c), the corresponding histidine is at position 86 (His86).

In the Swiss-Model, His85 (equivalent to His96 in 4LV4) is misaligned. It does not form the expected Pi-sulfur interaction and fails to establish the necessary hydrogen bonds. This misalignment and the lack of proper interactions diminish the functional resemblance to the 4LV4 structure. phyre model positions His86 (corresponding to His96 in 4LV4) somewhat closer to the desired conformation. However, it does not fully achieve the necessary hydrogen bonding with the two aspartic acids. The histidine's planar angle deviates, which is not observed in the experimental crystal structure.

The position and interactions of other critical amino acids, such as aspartic acids and glutamic acid, are also essential. In 4LV4, the two aspartic acids and one glutamic acid form critical hydrogen bonds within the active site, contributing to its functional conformation and stability. The corresponding amino acids in 4TO8 should maintain similar positions and interactions to ensure the active site remains functional after HCA binding. The Swiss-Model does not replicate the critical hydrogen bonds and interactions necessary for maintaining the active site's function. phyre model shows some approximation in replicating these hydrogen bonds but still falls short of fully reproducing the required interactions, affecting the active site's fidelity.

2) Model built from structure alignment

a) Comparative Analysis of HCA Binding in MRSA FBA Proteins 4TO8 and 4LV4

In the study of the MRSA FBA protein (PDB ID: 4TO8), the goal was to dock it with the known inhibitor HCA. However, the 4TO8 structure is incompatible to HCA. The active pocket structures of 4LV4 and 4TO8 are not well fitted (Figure 9a). In the 4LV4 structure, Glu161, His96, and His252 form key polar bonds with the ligand (Figure 9b). In contrast, the 4TO8 structure involves His86, His209, and Asn233 in forming key polar bonds with the ligand (Figure 9c). The only differences in the amino acid types between 4LV4 and 4TO8 are Asp276 and Asn233, which occupy the same positions. Both HCA and FLC exhibit dense interactions with the zinc ion within the active pocket, primarily through ionic bonds between the zinc ion and the hydroxyl groups on the ligand. The side chain angles of Glu161 and 137, which occupy the same position, differ by approximately 90 degrees. This discrepancy is likely due to differences between the FBAIIa and FBAIIb subtypes [100], which may influence the overall conformation and interaction dynamics within the active site.

b) Structural Modelling Challenges in Accommodating HCA in MRSaFBA (PDB ID: 4TO8) Compared to MtFBA (PDB ID: 4LV4)

To address this challenge, reference was made to the structure of MtFBA from another species (PDB ID: 4LV4) including HCA. Sequence alignment was initiated using Phyre2 and Swiss Model, incorporating the MRSaFBA sequence and the 4LV4 structure. The initial model did not align well with the active site of 4LV4 and was unable to accommodate HCA. Both the SwissModel and phyre model were found inadequate in accurately aligning critical residues, such as His85/His86, in MRSaFBA (PDB ID: 4TO8) with the reference protein (PDB ID: 4LV4), essential for accommodating the inhibitor HCA. Swiss-Model's misalignment led to the absence of expected Pi-sulfur interactions and key hydrogen bonds crucial for structural stability compared to 4LV4. While phyre model approached the correct conformation for His86, it failed to fully replicate necessary hydrogen bonds with surrounding residues and introduced non-native interactions. Additionally, both models did not accurately reproduce the specific hydrogen bonds involving critical residues like aspartic acids and glutamic acid observed in
4LV4, which are vital for maintaining the active site's functional stability.

c) Structural Refinement and Docking Analysis of 4TO8 to Mimic HCA Binding Mode in 4LV4

Using Pymol, chain A of 4TO8 was superimposed onto 4LV4 (RMSD = 0.940 for 162 atoms), followed by structural refinement in Coot to closely resemble 4LV4, involving the removal of residues 180-182 and 188-192 due to modelling challenges. The adjusted model underwent further refinement with Phyre2 to complete loops and improve geometry. Subsequent manual adjustments in Coot corrected sidechains in the active site, and the zinc ion from 4LV4 was integrated. The final model exhibited an RMSD of 0.246 for 164 atoms compared to 4LV4. For precise alignment, structure-based alignment of the final model with 4LV4 was conducted. Docking simulations using LeDock employed the HCA molecule retrieved from PubChem, converted to mol2 format with appropriate protonation states using Open Babel. The docking results revealed two primary clusters with scores of - 5.60 kcal/mol and -5.41 kcal/mol, respectively, with the second cluster closely resembling the HCA binding mode observed in 4LV4.

d) Comparative Assessment of Modelled Structure Accuracy and HCA Binding Mode Reproduction Using Molecular Docking

To evaluate the accuracy of the modelled structure and its ability to reproduce the binding mode of HCA in the experimental crystal, we re- docked HCA into the modelled structure using molecular docking. As shown in Figure d, the pose1 obtained from docking completely reproduces the binding mode of the ligand in the experimental crystal structure, confirming the reliability of the modelled structure. Figure e presents the pose2 of HCA docking, where the ligand binding mode differs from the experimental crystal but still forms hydrogen bonds with His86 and His209. Additionally, pose2 forms an extra hydrogen bond with Gly210 through the hydroxyl group.

These findings highlight the robustness of the docking methodology and suggest that the modelled structure can accurately mimic the experimental binding interactions of HCA. With this site, the PPF and CTCB libraries (containing 656 and 636 compounds respectively) of were docked to look for possible ligand binding. In the ligand screening process, in addition to energy and ligand efficiency scores, the main observation was the pose of the ligand. whether it can form hydrogen bonds with amino acids around the active site, and the coupling with zinc. The following eight ligands were screened out from a total of 1292 ligands in the two libraries for subsequent experiments (Table 2). Energy and Ligand Efficiency (LE)are used as scoring criteria: Energy values in molecular docking, such as binding energy or interaction energy, are typically expressed in kilocalories per mole (kcal/mol); Ligand Efficiency is a normalized metric that reflects the binding energy per atom of a ligand (kcal/mol/atom).

Table 2. Analysis of Ligand Binding Energies and Efficiencies for Selected PPF and CTCB Ligands with Protein Models; (A) Ligands selected from PPF (whose pose is similar to HCA pose 1 shown in Figure 9), (B) Ligands selected from PPF (whose pose is similar to f HCA pose 2 shown in Figure 9), (C) Ligands selected from CTCB.

(A) Ligands selected from PPF (whose pose is similar to HCA pose 1 shown in Figure 9)				
	PPF 68	PPF 462	PPF 654	HCA from 4LV4
Energy (kcal/mol)	-5.76	-3.38	-3.06	-5.63
Ligand Efficiency (kcal/mol/atom)	-0.32	-0.338	-0.34	-0.402
Structure	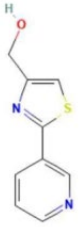	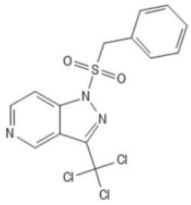	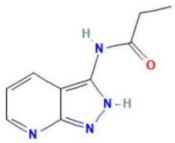	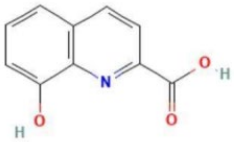

(B) Ligands selected from PPF (whose pose is similar to f HCA pose 2 shown in Figure 9)			
	PPF 161	PPF 349	PPF 486
Energy (kcal/mol)	-5.04	-5.49	-5.42
Ligand Efficiency (kcal/mol/atom)	-0.229	-0.275	-0.226
Structure	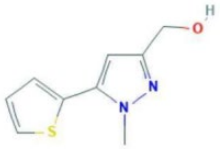	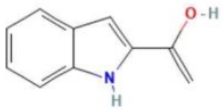	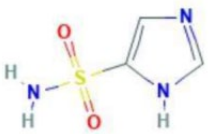

(C) Ligands selected from CTCB		
	CTCB 79	CTCB 82
Energy (kcal/mol)	-4.51	-3.42
Efficiency (kcal/mol/atom)	-0.301	-0.263
Structure	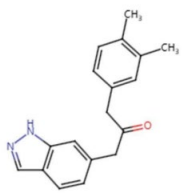	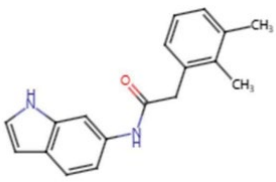

(e) Assessment of Ligand Efficacy and Binding Mechanisms in MRSaFBA Inhibition Studies

The experiment condition was built based on the establish of control group. For ligand obtained by docking, experiments were performed at substrate concentration (0.5 mM FBP) much smaller than the concentration at saturation, stable and reproducible enzyme concentrations, and certain zinc concentrations to optimize the curve rate and stability. Protein with DMSO was the control group.

Dimethyl sulfoxide (DMSO) is an organosulfur compound with the molecular formula (CH3)2SO, an important polar non-affinity solvent. Whereas, at high concentrations of dimethyl sulfoxide (DMSO), proteins may experience protein denaturation, which is caused by the breaking of hydrogen bonds within the protein and between the protein and water molecules by DMSO; protein aggregation, as DMSO alters the surface properties and hydrophobicity of proteins; and affects protein activity [25,101,102]. Therefore, when using DMSO in experiments, its concentration should be controlled as much as possible and the stability and activity of proteins in DMSO should be verified experimentally.

As shown in Figure 10, the inhibition rate of the protein with 1% DMSO compared to the MRSaFBA protein alone was calculated to be 73.4%, using the following formula: (%) = (1−2.057/7.736) × 100%, where 2.057 μmol·min^{-1}·mg^{-1} is the average specific enzyme activity of the protein with 1% DMSO, and 7.736 μmol·min^{-1}·mg^{-1} is the average specific enzyme activity of the MRSaFBA protein alone. Since the ligand for the subsequent study was dissolved in 100% DMSO, a 1% DMSO concentration was used as the control, requiring a 100-fold dilution of DMSO in the enzyme assay. HCA was used as a positive control, as it is a known inhibitor of MRSaFBA. At 1 mM, HCA resulted in a 62.4% inhibition compared to the control group, calculated as: (%) = (1−0.774/2.057) × 100%, where 2.057 μmol·min^{-1}·mg^{-1} is the average specific enzyme activity of the protein with 1% DMSO, and 0.774 μmol·min^{-1}·mg^{-1} is the average specific enzyme activity of the protein with HCA (The specific enzyme activity was calculated according to the calculation steps listed in the Method 2.2.3).

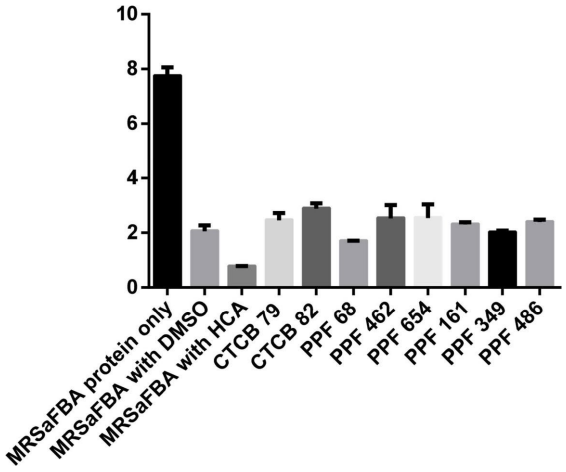

Figure 10. Comparative Analysis of MRSaFBA Enzyme Activity with Eight Ligands selected from CTCB and PPF Library, where the vertical coordinate is the specific enzyme activity (μmol·min-1·mg-1), the horizontal coordinate is the number of each ligand and the control group.

For the enzyme assays, triplicate experiments were conducted. For the ligands 79 and 82 screened from the CTCB library, assays were performed at a ligand concentration of 100 μM in 1% DMSO. For ligands 68, 462, and 654 screened from the PPF library, assays were conducted at a ligand concentration of 500 μM in 1% DMSO. For ligands 161, 349, and 486 from the PPF library, assays were performed at a ligand concentration of 1 mM in 1% DMSO. The screened ligands were compared to the control group (protein with 1% DMSO) as shown in Figure 10. The specific enzyme activity (μmol·min^{-1}·mg^{-1}) was plotted on the vertical axis, with the mean specific enzyme activity ± SD observed for each ligand. This comparison was used to determine whether the values overlapped with the control group's mean ± SD or if there was a significant difference.

From Figure 10, it is observed that ligand 68 from the PPF library, at a concentration of 500 μM, and detailed values represented by each column in Figure 10 are shown in Table 3. Therefore, comparing a specific enzyme activity of 1.694±0.017 μmol·min^{-1}·mg^{-1} (PPF 161) to the control group's 2.057±0.2134 μmol·min^{-1}·mg^{-1}, resulting in an inhibition

rate of approximately 18%. This difference remains statistically significant even when considering the SD. Table 3 below summarizes the specific enzyme activities and their respective variability for the MRSaFBA protein under various conditions and with different ligand，detailed calculation for specific enzyme activities can be seen in Method 2.2.3.

Table 3. Summary of MRSaFBA Enzyme Activities and Variability.

Sample Name	Mean Value ($\mu mol \cdot min^{-1} \cdot mg^{-1}$)	Standard Deviation ($\mu mol \cdot min^{-1} \cdot mg^{-1}$)
MRSaFBA protein only	7.736	0.330
MRSaFBA with DMSO	2.058	0.214
MRSaFBA with HCA	0.774	0.016
CTCB 79	2.453	0.265
CTCB 82	2.881	0.200
PPF 68	2.304	0.085
PPF 462.	2.014	0.068
PPF 654	2.398	0.085
PPF 161	1.694	0.017
PPF 349	2.530	0.484
PPF 486	2.541	0.498

The structure of PPF 68 is presented in the accompanying table, and its highest-scoring binding pose resembles that of HCA as seen in the 4LV4 structure. Based on its structure, the -CH2OH chain in PPF 68 may form hydrogen bonds with the -COOH group of Glu137, the same residue that interacts with HCA. Additionally, PPF 68 contains a pyridine ring and a thiazole ring. The nitrogen atoms in the pyridine ring, along with the nitrogen and sulfur atoms in the thiazole ring, can serve as coordination sites for zinc. Analysis of all binding poses suggests that PPF 68 is likely to form a bidentate coordination with zinc, involving the nitrogen from the pyridine ring and the sulfur from the thiazole ring, leading to a more stable complex [90]. The coordination of this ligand with zinc could be further visualized and confirmed through computational docking studies or experimental techniques such as X-ray crystallography or nuclear magnetic resonance spectroscopy to precisely detail the coordination geometry and interaction strength [94].

4. Conclusion

This article takes an in-depth look at the important enzyme MRSaFBA in the metabolism of MRSA. Using modified purification technologies, structural insights from DLS and TDA, and approaches for enzyme inhibition and molecular docking, we highlight the potential of MRSaFBA as an antibacterial target. These approaches deepen our understanding of the interaction of MRSaFBA with zinc and potential MRSAFBA-HCA sites. The demonstrated effect of different zinc concentrations on enzyme activity and structural integrity demonstrates the key role of zinc in regulating the activity and stability of class II FBAs--MRSaFBA. Studies have found that low concentrations of zinc increase the activity and stability of MRSaFBA, while high concentrations occupy activation sites and reduce substrate accessibility, thereby inhibiting enzyme activity. These results highlight the complex interactions between metal ions and enzyme functions and provide a reference for the design of experiments related to MRSaFBA activity.

Furthermore, based on this work, the MRSaFBA-HCA models derived from these studies have significant research value and deserve further study of their crystal structure. With a detailed crystallographic structure in place, expanding the screening of ligand libraries can lead to more comprehensive in vitro experiments. Subsequently, designing in vivo models to validate the therapeutic potential of confirmed inhibitors is recommended. Furthermore, broadening the scope of the study to include more diverse environmental

conditions and inhibitor molecules could reveal additional information about enzyme behavior and interactions, paving the way for precision medicine approaches in infectious disease treatment.

References

1. H. F. Wertheim, D. C. Melles, M. C. Vos, et al., "The role of nasal carriage in *Staphylococcus aureus* infections," *Lancet Infect. Dis.*, vol. 5, no. 12, pp. 751–762, 2005, doi: 10.1016/S1473-3099(05)70255-4.
2. D. J. Diekema, M. A. Pfaller, F. J. Schmitz, et al., "Survey of infections due to *Staphylococcus* species: frequency of occurrence and antimicrobial susceptibility of isolates collected in the United States, Canada, Latin America, Europe, and the Western Pacific region for the SENTRY Antimicrobial Surveillance Program, 1997–1999," *Clin. Infect. Dis.*, vol. 32 Suppl 2, pp. S114–S132, 2001, doi: 10.1086/323274.
3. A. S. Lee, H. de Lencastre, J. Garau, et al., "Methicillin-resistant *Staphylococcus aureus*," *Nat. Rev. Dis. Primers*, vol. 4, p. 18033, 2018, doi: 10.1038/s41572-018-0033-8.
4. F. D. Lowy, "*Staphylococcus aureus* infections," *N. Engl. J. Med.*, vol. 339, no. 8, pp. 520–532, 1998, doi: 10.1056/NEJM199808203390806.
5. S. A. Anuj, H. P. Gajera, D. G. Hirpara, et al., "Interruption in membrane permeability of drug-resistant *Staphylococcus aureus* with cationic particles of nano-silver," *Eur. J. Pharm. Sci.*, vol. 127, pp. 208–216, 2019, doi: 10.1056/NEJM199808203390806.
6. S. G. Zárate, P. Morales, K. Świderek, et al., "A molecular modeling approach to identify novel inhibitors of the major facilitator superfamily of efflux pump transporters," *Antibiotics*, vol. 8, no. 1, p. 13, 2019, doi: 10.1016/j.ejps.2018.12.014.
7. T. Matono, M. Nagashima, K. Mezaki, et al., "Molecular epidemiology of β-lactamase production in penicillin-susceptible *Staphylococcus aureus* under high-susceptibility conditions," *J. Infect. Chemother.*, vol. 24, no. 2, pp. 153–155, 2018, doi: 10.3390/antibiotics8010001.
8. L. Kime, C. P. Randall, F. I. Banda, et al., "Transient silencing of antibiotic resistance by mutation represents a significant potential source of unanticipated therapeutic failure," *mBio*, vol. 10, no. 5, pp. 1–13, 2019, doi: 10.1016/j.jiac.2017.11.005.
9. R. Kanwari, A. K. Sah, and P. Suresh, "Biofilm-mediated antibiotic-resistant oral bacterial infection," *Curr. Drug Targets*, doi: 10.2174/1381612822666161124154549.
10. A. F. Haag, J. R. Fitzgerald, J. R. Penadés, et al., "*Staphylococcus aureus* in animals," *Microbiol. Spectr.*, vol. 7, no. 3, p. GPP3-0060-2019, 2019, doi: 10.1128/microbiolspec.GPP3-0060-2019.
11. A. Fetsch and S. Johler, "*Staphylococcus aureus* as a foodborne pathogen," *Curr. Clin. Microbiol. Rep.*, vol. 5, no. 2, pp. 88–96, 2018, doi: 10.1007/s40588-018-0111-2.
12. B. Sancak, "*Staphylococcus aureus* and antibiotic resistance," *Mikrobiyol. Bul.*, vol. 45, no. 3, pp. 565–576, 2011, doi: 10.5402/2011/812049.
13. D. Lim and N. C. Strynadka, "Structural basis for the β-lactam resistance of PBP2a from methicillin-resistant *Staphylococcus aureus*," *Nat. Struct. Biol.*, vol. 9, no. 11, pp. 870–876, 2002, doi: 10.1038/nsb813.
14. K. A. Lacey, J. A. Geoghegan, and R. M. McLoughlin, "The role of *Staphylococcus aureus* virulence factors in skin infection and their potential as vaccine antigens," *Pathogens*, vol. 5, no. 1, p. 22, 2016, doi: 10.3390/pathogens5010022.
15. L. Tuchscherr, B. Löffler, and R. A. Proctor, "Persistence of *Staphylococcus aureus*: multiple metabolic pathways impact the expression of virulence factors in small-colony variants (SCVs)," *Front. Microbiol.*, vol. 11, p. 1028, 2020, doi: 10.3389/fmicb.2020.01028.
16. A. E. Paharik and A. R. Horswill, "The staphylococcal biofilm: adhesins, regulation, and host response," *Microbiol. Spectr.*, vol. 4, no. 2, p. VMBF-0022-2015, 2016, doi: 10.1128/microbiolspec.VMBF-0022-2015.
17. R. M. Donlan, "Biofilms: microbial life on surfaces," *Emerg. Infect. Dis.*, vol. 8, no. 9, p. 881, 2002, doi: 10.3201/eid0809.020063.
18. G. Y. C. Cheung, J. S. Bae, and M. Otto, "Pathogenicity and virulence of *Staphylococcus aureus*," *Virulence*, vol. 12, no. 1, pp. 547–569, 2021, doi: 10.1080/21505594.2020.1839562.
19. K. Tam, V. J. Torres, V. A. Fischetti, *et al.*, "*Staphylococcus aureus* secreted toxins and extracellular enzymes," *Microbiol. Spectr.*, vol. 7, no. 2, p. GPP3-0039-2018, 2019, doi: 10.1128/microbiolspec.GPP3-0039-2018.
20. S. Divyakolu, R. Chikkala, K. S. Ratnakar, *et al.*, "Hemolysins of *Staphylococcus aureus*—an update on their biology, role in pathogenesis and as targets for antivirulence therapy," *Adv. Infect. Dis.*, vol. 9, no. 2, pp. 80–104, 2019, doi: 10.1155/2019/6483049.
21. C. Liu, Y. Shen, M. Yang, *et al.*, "Hazard of staphylococcal enterotoxins in food and promising strategies for natural products against virulence," *J. Agric. Food Chem.*, vol. 70, no. 8, pp. 2450–2465, 2022, doi: 10.1021/acs.jafc.1c07141.
22. J. K. McCormick, J. M. Yarwood, and P. M. Schlievert, "Toxic shock syndrome and bacterial superantigens: an update," *Annu. Rev. Microbiol.*, vol. 55, no. 1, pp. 77–104, 2001, doi: 10.1146/annurev.micro.55.1.77.
23. A. Sakr, F. Bregeon, J.-L. Mege, *et al.*, "*Staphylococcus aureus* nasal colonization: an update on mechanisms, epidemiology, risk factors, and subsequent infections," *Front. Microbiol.*, vol. 9, p. 2419, 2018, doi: 10.3389/fmicb.2018.02419.
24. L. G. Bode, J. A. Kluytmans, H. F. Wertheim, *et al.*, "Preventing surgical-site infections in nasal carriers of *Staphylococcus aureus*," *N. Engl. J. Med.*, vol. 362, no. 1, pp. 9–17, 2010, doi: 10.1056/NEJMoa0808939.

25. H. Dixit, M. Kulharia, and S. K. Verma, "Metal-binding proteins and proteases in RNA viruses: unravelling functional diversity and expanding therapeutic horizons," *J. Virol.*, vol. 97, no. 12, e0139923, Dec. 2023, doi: 10.1128/jvi.01399-23.
26. S. S. Huang, R. Singh, J. A. McKinnell, *et al.*, "Decolonization to reduce postdischarge infection risk among MRSA carriers," *N. Engl. J. Med.*, vol. 380, no. 7, pp. 638–650, 2019, doi: 10.1056/NEJMoa1810913.
27. A. Hamdan-Partida, S. Gonzalez-Garcia, E. de la Rosa Garcia, *et al.*, "Community acquired methicillin-resistant *Staphylococcus aureus* can persist in the throat," *Int. J. Med. Microbiol.*, vol. 308, no. 4, pp. 469–475, 2018, doi: 10.1016/j.ijmm.2018.04.002.
28. I. S. Petersen, P. L. Larsen, B. L. Brandelev, *et al.*, "Close association between oropharyngeal and rhinopharyngeal colonization with *Staphylococcus aureus* – clues to new insight of MRSA colonization of the oropharynx," *J. Hosp. Infect.*, vol. 84, no. 3, pp. 259–262, 2013, doi: 10.1016/j.jhin.2013.04.007.
29. E. S. Yang, J. Tan, S. Eells, *et al.*, "Body site colonization in patients with community-associated methicillin-resistant *Staphylococcus aureus* and other types of *S. aureus* skin infections," *Clin. Microbiol. Infect.*, vol. 16, no. 5, pp. 425–431, 2010, doi: 10.1111/j.1469-0691.2009.02836.
30. D. S. Acton, M. J. Tempelmans Plat-Sinnige, W. van Wamel, *et al.*, "Intestinal carriage of *Staphylococcus aureus*: how does its frequency compare with that of nasal carriage and what is its clinical impact?" *Eur. J. Clin. Microbiol. Infect. Dis.*, vol. 28, no. 2, p. 115, 2008, doi: 10.1007/s10096-007-0384-6.
31. D. M. Gries, N. J. Pultz, and C. J. Donskey, "Growth in cecal mucus facilitates colonization of the mouse intestinal tract by methicillin-resistant *Staphylococcus aureus*," *J. Infect. Dis.*, vol. 192, no. 9, pp. 1621–1627, 2005, doi: 10.1086/430464.
32. T. S. Lo and S. M. Borchardt, "Antibiotic-associated diarrhea due to methicillin resistant *Staphylococcus aureus*," *Diagn. Microbiol. Infect. Dis.*, vol. 63, no. 4, pp. 388–389, 2009, doi: 10.1016/j.diagmicrobio.2008.12.007.
33. M. Y. Khan and W. H. Hall, "Staphylococcal enterocolitis—treatment with oral vancomycin," *Ann. Intern. Med.*, vol. 65, no. 1, pp. 1–8, 1966, doi: 10.7326/0003-4819-65-1-1.
34. M. A. Krezalek, S. Hyoju, A. Zaborin, et al., "Can methicillin-resistant *Staphylococcus aureus* silently travel from the gut to the wound and cause postoperative infection? Modeling the 'Trojan Horse Hypothesis'," *Ann. Surg.*, vol. 267, no. 4, pp. 749–758, 2018, doi: 10.1097/SLA.0000000000002173.
35. E. J. Raineri, D. Altulea, and J. M. van Dijl, "Staphylococcal trafficking and infection—from 'nose to gut' and back," *FEMS Microbiol. Rev.*, vol. 46, no. 1, p. fuab041, 2021, doi: 10.1093/femsre/fuab041.
36. C.-J. Yao, Y.-L. Li, M.-J. Pu, *et al.*, "Aminoglycosides with anti-MRSA activity: a concise review," *Curr. Top. Med. Chem.*, vol. 21, no. 27, pp. 2483–2499, 2021, doi: 10.2174/1568026621666211004093647.
37. T. Yamamichi, M. Yoshida, T. Sakai, *et al.*, "Factors associated with neonatal surgical site infection after abdominal surgery," *Pediatr. Surg. Int.*, vol. 38, no. 2, pp. 317–323, 2022, doi: 10.1007/s00383-021-05051-5.
38. C.-M. Yueh, H. Chi, N.-C. Chiu, *et al.*, "Etiology, clinical features, management, and outcomes of skin and soft tissue infections in hospitalized children: A 10-year review," *J. Microbiol. Immunol. Infect.*, vol. 55, no. 4, pp. 728–739, 2022, doi: 10.1016/j.jmii.2022.01.007.
39. S. Alosaimy, N. L. Sabagha, A. M. Lagnf, *et al.*, "Monotherapy with vancomycin or daptomycin versus combination therapy with beta-lactams in the treatment of methicillin-resistant *Staphylococcus aureus* bloodstream infections: a retrospective cohort analysis," *Infect. Dis. Ther.*, vol. 9, no. 2, pp. 325–339, 2020, doi: 10.1007/s40121-020-00292-8.
40. W. Abebe, B. Tegene, T. Feleke, *et al.*, "Bacterial bloodstream infections and their antimicrobial susceptibility patterns in children and adults in Ethiopia: a 6-year retrospective study," *Clin. Lab.*, vol. 67, no. 11, pp. 2453–2461, 2021, doi: 10.7754/Clin.Lab.2021.210224.
41. S. Arakawa, M. Kasai, S. Kawai, *et al.*, "The JAID/JSC guidelines for management of infectious diseases 2017—Sepsis and catheter-related bloodstream infection," *J. Infect. Chemother.*, vol. 27, no. 5, pp. 657–677, 2021, doi: 10.1016/j.jiac.2019.11.011.
42. M. Anvarinejad, M. Khalifeh, J. Mardaneh, *et al.*, "Bloodstream infections in the south of Iran: microbiological profile and antibiotic-resistance patterns of isolated bacteria," *Crescent J. Med. Biol. Sci.*, vol. 8, no. 4, pp. 312–318, 2021.
43. V. Agrawal, A. T. Valson, Y. D. Bakthavatchalam, *et al.*, "Skin colonizers and catheter associated blood stream infections in incident Indian dialysis patients," *Indian J. Nephrol.*, vol. 32, no. 1, pp. 34–41, 2022, doi: 10.4103/ijn.IJN_400_20.
44. S.-S. Jean, Y.-C. Chang, W.-C. Lin, *et al.*, "Epidemiology, treatment, and prevention of nosocomial bacterial pneumonia," *J. Clin. Med.*, vol. 9, no. 1, p. 275, 2020, doi: 10.3390/jcm9010275.
45. M. S. Soliman, N. S. Soliman, A. R. El-Manakhly, *et al.*, "Genomic characterization of methicillin-resistant *Staphylococcus aureus* (MRSA) by high-throughput sequencing in a tertiary care hospital," *Genes*, vol. 11, no. 10, p. 1219, 2020, doi: 10.3390/genes11101219.
46. M. Ohlmeier, S. Filitarin, G. Delgado, *et al.*, "Improved treatment strategies can result in better outcomes following one-stage exchange surgery for MRSA periprosthetic joint infection," *J. Med. Microbiol.*, vol. 69, no. 8, 2020, doi: 10.1099/jmm.0.001229.
47. A. Ou, K. Wang, Y. Mao, *et al.*, "First report on the rapid detection and identification of methicillin-resistant *Staphylococcus aureus* (MRSA) in viable but non-culturable (VBNC) under food storage conditions," *Front. Microbiol.*, vol. 11, 2021, doi: 10.3389/fmicb.2020.615875.

48. A. Alabresm, Y. P. Chen, S. Wichter-Chandler, *et al.*, "Nanoparticles as antibiotic-delivery vehicles (ADVs) overcome resistance by MRSA and other MDR bacterial pathogens: The grenade hypothesis," *J. Glob. Antimicrob. Resist.*, vol. 22, 2020, doi: 10.1016/j.jgar.2020.06.023.
49. G. Gagandeep, P. Kumar, S. K. Kandi, *et al.*, "Synthesis of novel monocarbonyl curcuminoids, evaluation of their efficacy against MRSA, including ex vivo infection model and their mechanistic studies," *Eur. J. Med. Chem.*, vol. 195, p. 112276, 2020, doi: 10.1016/j.ejmech.2020.112276.
50. G. K. Paterson, "Low prevalence of livestock associated methicillin-resistant *Staphylococcus aureus* clonal complex 398 and mecC MRSA among human isolates in Northeast England," *J. Appl. Microbiol.*, vol. 128, no. 6, 2020, doi: 10.1111/jam.14578.
51. Y. Qiao, X. Liu, B. Li, *et al.*, "Treatment of MRSA-infected osteomyelitis using bacterial capturing, magnetically targeted composites with microwave-assisted bacterial killing," *Nat. Commun.*, vol. 11, no. 1, p. 4446, 2020, doi: 10.1038/s41467-020-18271-4.
52. B. T. M. J. A., B. K. C. M. A., B. M. A. M. A., *et al.*, "Combination ceftaroline and daptomycin salvage therapy for complicated methicillin-resistant *Staphylococcus aureus* (MRSA) bacteremia compared with standard of care," *Int. J. Antimicrob. Agents*, 2021, doi: 10.1016/j.ijantimicag.2021.106310.
53. D. C. Coleman, A. C. Shore, R. V. Goering, *et al.*, "New insights and updates on the molecular epidemiology and antimicrobial resistance of MRSA in humans in the whole genome sequencing era," *Front. Microbiol.*, vol. 10, 2019, p. 637, doi: 10.3389/fmicb.2019.00637.
54. S. H. Kuo, C. S. Chien, C. C. Wang, *et al.*, "Antibacterial activity of BSA-capped gold nanoclusters against methicillin-resistant *Staphylococcus aureus* (MRSA) and vancomycin intermediate *Staphylococcus aureus* (VISA)," *J. Nanomater.*, vol. 2019, pp. 1–7, 2019, doi:.
55. S.-C. Yang, K.-W. Shih, *et al.*, "Discovery of furanoquinone derivatives as a novel class of DNA polymerase and gyrase inhibitors for MRSA eradication in cutaneous infection," *Front. Microbiol.*, vol. 10, p. 1197, 2019, doi: 10.3389/fmicb.2019.01197.
56. G.-Y. Zuo, C.-X. Cui, *et al.*, "Potent anti-MRSA activity and synergism with aminoglycosides by flavonoid derivatives from the root barks of *Morus alba*, a traditional Chinese medicine," *Med. Chem. Res.*, vol. 28, no. 9, pp. 1547–1556, 2019, doi: 10.1007/s00044-019-02393-7.
57. B. Chen, "Molecular mechanism of HIV-1 entry," *Trends Microbiol.*, vol. 27, no. 10, pp. 878–891, 2019, doi: 10.1016/j.tim.2019.06.002.
58. M. R. S. A. Janjua, "Structure–property relationship and systematic study of a series of terpyridine-based nonlinear optical compounds: DFT computation of interactive design," *J. Cluster Sci.*, vol. 30, no. 1, pp. 45–51, 2019, doi: 10.1007/s10876-018-1445-6.
59. C. D. de Morais Oliveira-Tintino, S. R. Tintino, D. F. Muniz, *et al.*, "Do 1,8 naphthyridine sulfonamides possess an inhibitory action against TetK and MrsA efflux pumps in multiresistant *Staphylococcus aureus* strains?" *Microb. Pathog.*, vol. 147, p. 104268, 2020, doi: 10.1016/j.micpath.2020.104268.
60. J. K. Ferguson, S. A. Munnoch, K. Kozierowski, *et al.*, "Reduced VRE and MRSA colonisation and infection following sustained reduction in broad spectrum antibiotic use in a large tertiary hospital," *Med. J. Aust.*, vol. 211, no. 3, 2019, doi: 10.5694/mja2.50218.
61. F. Gu, W. He, S. Xiao, *et al.*, "Antimicrobial resistance and molecular epidemiology of *Staphylococcus aureus* causing bloodstream infections at Ruijin Hospital in Shanghai from 2013 to 2018," *Sci. Rep.*, vol. 10, no. 1, 2020, doi: 10.1038/s41598-020-62444-1.
62. Yao, Chen, Yuan, *et al.*, "Design, synthesis, and antibacterial evaluation of novel derivatives of NPS-2143 for the treatment of methicillin-resistant *S. aureus* (MRSA) infection," *J. Antibiotics*, 2019, doi: 10.1038/s41429-019-0177-9.
63. Y. W. Chang, W. C. Huang, C. Y. Lin, *et al.*, "Tellimagrandin II, a type of plant polyphenol extracted from *Trapa bispinosa* inhibits antibiotic resistance of drug-resistant *Staphylococcus aureus*," *Int. J. Mol. Sci.*, vol. 20, no. 22, 2019, doi: 10.3390/ijms20225666.
64. A. Alberto, T. G. Tommaso, M. C. Marco, *et al.*, "Staphylococcus aureus from hospital-acquired pneumonia from an Italian nationwide survey: Activity of ceftobiprole and other anti-staphylococcal agents, and molecular epidemiology of methicillin-resistant isolates," *J. Antimicrob. Chemother.*, no. 12, 2019, doi: 10.1093/jac/dkz371.
65. B. K. G. Eriksson, U.-B. Thollström, J. Nederby-Öhd, *et al.*, "Epidemiology and control of meticillin-resistant *Staphylococcus aureus* in Stockholm County, Sweden, 2000 to 2016: Overview of a 'search-and-contain' strategy," *Eur. J. Clin. Microbiol. Infect. Dis.*, vol. 38, no. 12, pp. 2221–2228, 2019, doi: 10.1007/s10096-019-03622-6.
66. K. O. Kwok, E. Chan, P. H. Chung, *et al.*, "Prevalence and associated factors for carriage of Enterobacteriaceae producing ESBLs or carbapenemase and methicillin-resistant *Staphylococcus aureus* in Hong Kong community," *J. Infect.*, vol. 81, no. 2, pp. 242-247, 2020, doi: 10.1016/j.jinf.2020.05.033.
67. H. Wang, C.-R. Chung, Z. Wang, S. Li, B.-Y. Chu, J.-T. Horng, J.-J. Lu, and T.-Y. Lee, "A large-scale investigation and identification of methicillin-resistant *Staphylococcus aureus* based on peaks binning of matrix-assisted laser desorption ionization-time of flight MS spectra," *Brief. Bioinform.*, vol. 22, no. 3, 2021, doi: 10.1093/bib/bbaa138.
68. S. Zheng, S. J. Chung, H. C. J. Sim, *et al.*, "Impact of formulary interventions on the minimum inhibitory concentration of methicillin-resistant *Staphylococcus aureus* to mupirocin, chlorhexidine, and octenidine in a Singapore tertiary institution," *Eur. J. Clin. Microbiol. Infect. Dis.*, vol. 39, pp. 2397–2403, 2020, doi: 10.1007/s10096-020-03814-6.
69. B. Onowska, J. Sawiński, K. Garbacz, *et al.*, "N-(2-Arylmethylthio-4-chloro-5-methylbenzenesulfonyl)amide derivatives as potential antimicrobial agents—Synthesis and biological studies," *Int. J. Mol. Sci.*, vol. 21, no. 1, 2020, doi: 10.3390/ijms21010161.

70. H. Chen, Y. Yin, X. Li, S. Li, H. Gao, X. Wang, Y. Zhang, Y. Liu, and H. Wang, "Whole-genome analysis of livestock-associated methicillin-resistant *Staphylococcus aureus* sequence type 398 strains isolated from patients with bacteremia in China," *J. Infect. Dis.*, vol. 221, no. Suppl. 2, pp. S220–S228, 2020, doi: 10.1093/infdis/jiz575.
71. Y. D. Bakthavatchalam, A. Shankar, R. Muniyasamy, J. V. Peter, M. Zervos, H. T. Dwarakanathan, K. Gunasekaran, R. Iyadurai, and B. Veeraraghavan, "Levonadifloxacin, a recently approved benzoquinolizine fluoroquinolone, exhibits potent *in vitro* activity against contemporary *Staphylococcus aureus* isolates and Bengal Bay clone isolates collected from a large Indian tertiary care hospital," *J. Antimicrob. Chemother.*, vol. 75, no. 8, pp. 2156–2159, 2020, doi: 10.1093/jac/dkaa142.
72. P. Awolade, N. Cele, E. O. Ebenezer, *et al.*, "Synthesis of 1H-1,2,3-Triazole-linked quinoline isatin molecular hybrids as anti-breast cancer and anti-methicillin-resistant *Staphylococcus aureus* (MRSA) agents," *Anti-Cancer Agents Med. Chem.*, vol. 20, no. 10, pp. 1228-1239, 2020, doi: 10.2174/1871520620666200929153138.
73. L. A. Kelley, S. Mezulis, C. M. Yates, M. N. Wass, and M. J. Sternberg, "The Phyre2 web portal for protein modelling, prediction and analysis," *Nat. Protoc.*, vol. 10, no. 6, pp. 845–858, 2015, doi: 10.1038/nprot.2015.053.
74. E. Lorentzen, B. Siebers, R. Hensel, and E. Pohl, "Mechanism of the Schiff base forming fructose-1,6-bisphosphate aldolase: Structural analysis of reaction intermediates," *Biochemistry*, vol. 44, pp. 4222–4229, 2005, doi: 10.1021/bi050157n.
75. S. Zgiby, A. R. Plater, M. A. Bates, G. J. Thomson, and A. Berry, "A functional role for a flexible loop containing Glu182 in the class II fructose-1,6-bisphosphate aldolase from *Escherichia coli*," *J. Mol. Biol.*, vol. 315, no. 2, pp. 131–140, 2002, doi: 10.1006/jmbi.2001.5237.
76. A. Galkin, L. Kulakova, E. Melamud, L. Li, C. Wu, P. Mariano, D. Dunaway-Mariano, T. E. Nash, and O. Herzberg, "Characterization, kinetics, and crystal structures of fructose-1,6-bisphosphate aldolase from the human parasite, *Giardia lamblia*," *J. Biol. Chem.*, vol. 282, pp. 4859–4867, 2007, doi: 10.1074/jbc.M609121200.
77. S. Y. Gerdes, M. D. Scholle, J. W. Campbell, G. Balazsi, E. Ravasz, M. D. Daugherty, *et al.*, "Experimental determination and system level analysis of essential genes in *Escherichia coli* MG1655," *J. Bacteriol.*, vol. 185, pp. 5673–5684, 2003, doi: 10.1128/JB.185.19.5673-5684.2003.
78. E. O. Davis, M. C. Jones-Mortimer, and P. J. Henderson, "Location of a structural gene for xyloseH+ symport at 91 min on the linkage map of *Escherichia coli* K12," *J. Biol. Chem.*, vol. 259, pp. 1520–1525, 1984, doi: 10.1016/S0021-9258(18)43454-1.
79. I. Rosenkrands, R. A. Slayden, J. Crawford, C. Aagaard, C. E. 3rd Barry, and P. H. Andersen, "Hypoxic response of *Mycobacterium tuberculosis* studied by metabolic labeling and proteome analysis of cellular and extracellular proteins," *J. Bacteriol.*, vol. 184, pp. 3485–3491, 2002, doi: 10.1128/JB.184.12.3485-3491.2002.
80. K. Huynh and C. L. Partch, "Analysis of protein stability and ligand interactions by thermal shift assay," *Curr. Protoc. Protein Sci.*, vol. 79, pp. 28.9.1–28.9.14, 2015, doi: 10.1002/0471140864.ps2809s79.
81. G. C. Capodagli, S. A. Lee, K. J. Boehm, K. M. Brady, and S. D. Pegan, "Structural and functional characterization of methicillin-resistant *Staphylococcus aureus*'s class IIb fructose 1,6-bisphosphate aldolase," *Biochemistry*, vol. 53, no. 48, pp. 7604–7614, Dec. 2014, doi: 10.1021/bi501141t.
82. M. Shehadul Islam, A. Aryasomayajula, and P. R. Selvaganapathy, "A review on macroscale and microscale cell lysis methods," *Micromachines*, vol. 8, no. 3, p. 83, 2017, doi: 10.3390/mi8030083.
83. K. Gangele and K. M. Poluri, "Imidazole derivatives differentially destabilize the low pH conformation of lysozyme through weak electrostatic interactions," *RSC Adv.*, vol. 10, p. 1039, 2016, doi: 10.1039/C6RA23031H.
84. M. Tataruch, *et al.*, "Catalytic stability of S-1-(4-hydroxyphenyl)-ethanol dehydrogenase from *Aromatoleum aromaticum*," *Int. J. Mol. Sci.*, vol. 25, no. 13, 2024, doi: 10.3390/ijms25137385.
85. Q. Zhang, *et al.*, "Interaction mechanism and compatibility studies of silk protein peptide (SPP) with the common surfactants SDS and DTAB," *Spectrochim. Acta A Mol. Biomol. Spectrosc.*, vol. 322, p. 124833, 2024, doi: 10.1016/j.saa.2024.124833.
86. B. Van den Wouwer, *et al.*, "The effect of ultrasound on the extraction and foaming properties of proteins from potato trimmings," *Food Chem.*, vol. 455, p. 139877, 2024, doi: 10.1016/j.foodchem.2024.139877.
87. N. Nawaz, *et al.*, "Lysozyme and its application as antibacterial agent in food industry," *Molecules*, vol. 27, no. 19, 2022, doi: 10.3390/molecules27196305.
88. A. Flourieusse, *et al.*, "Formation of intracellular vesicles within the Gram (+) *Lactococcus lactis* induced by the overexpression of Caveolin-1beta," *Microb. Cell Fact.*, vol. 21, p. 239, 2022, doi: 10.1186/s12934-022-01944-9.
89. G. Salvi, P. De Los Rios, and M. Vendruscolo, "Effective interactions between chaotropic agents and proteins," *Proteins*, vol. 61, no. 3, pp. 492–499, Nov. 2005, doi: 10.1002/prot.20626.
90. G. C. Capodagli, W. G. Sedhom, M. Jackson, K. A. Ahrendt, and S. D. Pegan, "A noncompetitive inhibitor for *Mycobacterium tuberculosis*'s class IIa fructose-1,6-bisphosphate aldolase," *Biochemistry*, vol. 53, no. 1, pp. 202–213, Jan. 2014, doi: 10.1021/bi401022b.
91. A. Waterhouse, M. Bertoni, S. Bienert, G. Tauriello, R. Gumienny, T. Schwede, "SWISS-MODEL: homology modelling of protein structures and complexes," *Nucleic Acids Res.*, vol. 46, no. W1, pp. W296–W303, 2018, doi: 10.1093/nar/gky427.
92. K. Palanisamy, M. Prakash, and V. Rajapandian, "Combined DFT and MD simulation studies of protein stability on imidazolium–water (ImH+Wn) clusters with aromatic amino acids," *New J. Chem.*, vol. 44, pp. 17912–17923, 2020, doi: 10.1039/D0NJ03085F.

93. M. de la Paz Santangelo, *et al.*, "Glycolytic and non-glycolytic functions of *Mycobacterium tuberculosis* fructose-1,6-bisphosphate aldolase, an essential enzyme produced by replicating and non-replicating bacilli," *J. Biol. Chem.*, vol. 286, pp. 40219–40231, 2011, doi: 10.1074/jbc.M111.259440.
94. A. Waterhouse, M. Bertoni, S. Bienert, G. Tauriello, R. Gumienny, T. Schwede, "SWISS-MODEL: homology modelling of protein structures and complexes," *Nucleic Acids Res.*, vol. 46, no. W1, pp. W296–W303, 2018, doi: 10.1093/nar/gky427.
95. J. Schulze Wischeler, A. Innocenti, D. Vullo, A. Agrawal, S. M. Cohen, A. Heine, C. T. Supuran, and G. Klebe, "Bidentate zinc chelators for alpha-carbonic anhydrases that produce a trigonal bipyramidal coordination geometry," *ChemMedChem*, vol. 5, no. 9, pp. 1609–1615, Sep. 2010, doi: 10.1002/cmdc.201000200.
96. P. J. Mahanta and K. Lhouvum, "Expression and biochemical characterization of the putative insulinase enzyme PF11_0189 found in the *Plasmodium falciparum* genome," *Protein Expr. Purif.*, vol. 222, p. 106539, 2024, doi: 10.1016/j.pep.2024.106539.
97. S. Gu, *et al.*, "Expression and functional analysis of the metallothionein and metal-responsive transcription factor 1 in *Phascolosoma esculenta* under Zn stress," *Int. J. Mol. Sci.*, vol. 25, no. 13, 2024, doi: 10.3390/ijms25137368.
98. K. Varnagy, *et al.*, "Complex formation and hydrolytic processes of protected peptides containing the -SXH- motif in the presence of nickel (II) ion," *Chembiochem*, vol. 25, no. 20, e202400475, 2024, doi: 10.1002/cbic.202400475.
99. D. A. Gonzalez, *et al.*, "Preparation and characterization of Zn (II)-stabilized Abeta (42) oligomers," *ACS Chem. Neurosci.*, vol. 15, no. 14, pp. 2586–2599, 2024, doi: 10.1021/acschemneuro.4c00084.
100. A. Scozzafava and C. T. Supuran, "Hydroxyurea is a carbonic anhydrase inhibitor," *Bioorg. Med. Chem.*, vol. 11, no. 10, pp. 2241–2246, 2003, doi: 10.1016/S0968-0896(03)00112-3.
101. M. Glavare, M. Löfgren, and M. L. Schult, "Between unemployment and employment: experience of unemployed long-term pain sufferers," *Work*, vol. 43, no. 4, pp. 475–485, 2012, doi: 10.3233/WOR-2012-1394.
102. Y. Y. Chou, R. Vafabakhsh, S. Doğanay, Q. Gao, T. Ha, and P. Palese, "One influenza virus particle packages eight unique viral RNAs as shown by FISH analysis," *Proc. Natl. Acad. Sci. U.S.A.*, vol. 109, no. 23, pp. 9101–9106, Jun. 2012, doi: 10.1073/pnas.1206069109.